LncRNA *TAAL* is a Modulator of *Tie1*-Mediated Vascular Function in Diabetic Retinopathy

Gyan Ranjan[1,2 *], Samriddhi Arora[1], Sarmeela Sharma[3], Lakshita Sharma[2], Rahul C Bhoyar[2], Vigneshwar Senthivel[2], Vinod Scaria[2, 4, 5], Subhabrata Chakrabarti[3], Inderjeet Kaur[3], Sridhar Sivasubbu[2, 4, 5 *], Rajender K Motiani[1,*]

[1] Laboratory of Calciomics and Systemic Pathophysiology, Regional Center for Biotechnology (RCB), Faridabad, India.
[2] CSIR Institute of Genomics and Integrative Biology, New Delhi, India.
[3] Brien Holden Eye Research Centre L V Prasad Eye Institute Hyderabad, India.
[4] Vishwanath Cancer Care Foundation, Mumbai, India.
[5] Dr. D. Y Patil Medical College, Hospital and Research Centre, Pune, India.

*Corresponding authors:-

Dr. Gyan Ranjan
Postdoctoral Research Associate - Regional Centre for Biotechnology (RCB)
Faridabad, Delhi-NCR, India
Email: gyanranjan2197@gmail.com; gyan.ranjan@rcb.res.in

Dr. Rajender K Motiani
Associate Professor - Regional Centre for Biotechnology (RCB)
Faridabad, Delhi-NCR, India
Email: rajender.motiani@rcb.res.in

Dr. Sridhar Sivasubbu
Chief Scientist, CSIR Institute of Genomics and Integrative Biology (CSIR-IGIB),
New Delhi, India
Present address:
Senior Consultant, Vishwanath Cancer Care Foundation, Mumbai, India
Adjunct Professor, Dr. D. Y Patil Medical College, Hospital and Research Centre, Pune, India
Email: sridhar@igib.in ; sridhar.sivasubbu@gmail.com

Abstract.

Diabetic retinopathy (DR) is a leading cause of vision impairment and blindness resulting from abnormal retinal vascular changes due to chronic hyperglycemia. The *ANG-TIE* signaling pathway, crucial for vascular growth and remodeling, is a key therapeutic target in DR. Through a protein-centric approach, we identified a novel lncRNA an named it *Tie1-associated angiogenic lncRNA (TAAL)*, which regulates endothelial cell migration, proliferation, tube formation, permeability, and angiogenesis via changing calcium and cytoskeleton dynamics in endothelial cells. In zebrafish, modulation of the *TAAL* orthologue led to angiogenic defects, which were rescued by human *TAAL*. Molecular studies revealed that *TAAL* negatively regulates *Tie1* protein expression through ubiquitin-mediated degradation. Notably, *TAAL* is upregulated in the blood of DR patients and is reduced in endothelial DR cell models. Overexpression of *TAAL* restores permeability and VE-cadherin surface expression. These findings present a novel function of lncRNA *TAAL* as a critical regulator of *Tie1* protein turnover with potential therapeutic applications for diabetic retinopathy.

Keywords

lncRNA, Diabetic Retinopathy, Tie1, endothelial, zebrafish, permeability, vascular

Synopsis

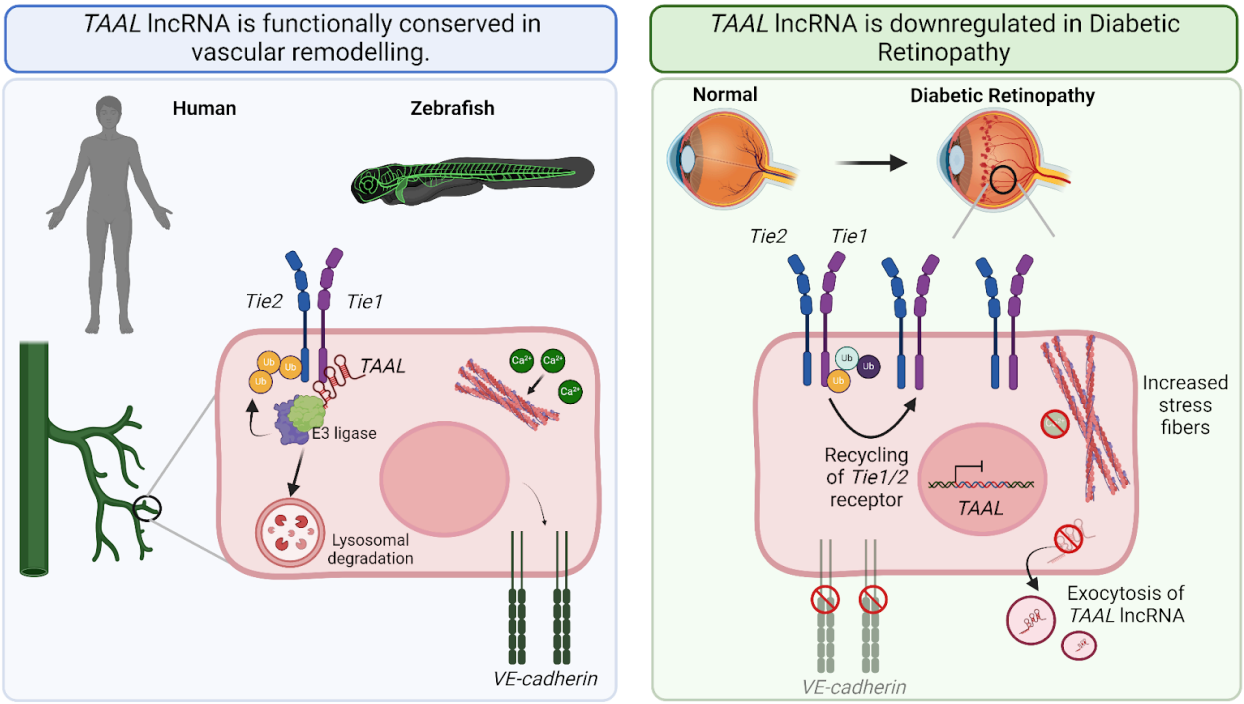

Tie1 is an endothelial protein that plays a critical role in neovascularization. Its interactome is not well studied. Here, we discover a novel lncRNA *TAAL* that interacts with *Tie1* protein and regulates its protein turnover thereby, *TAAL* modulates endothelial pathophysiology.

- The *TAAL* lncRNA interacts with the *Tie1* protein and regulates vascular remodeling.
- The *TAAL* lncRNA is functionally conserved between human and zebrafish. It plays an important role in regulating vascular angiogenesis during development.
- The *TAAL* lncRNA controls the protein turnover of *Tie1* by ubiquitin-mediated modulation of its stabilization and translation.
- The *TAAL* lncRNA is hyperactive during diabetic retinopathy and is a potential biomarker and a potent therapeutic target.

Introduction

Diabetes mellitus (DM) is a chronic metabolic disorder characterized by persistent hyperglycemia, which can have detrimental effects on multiple organs, including the kidneys, liver, and cardiovascular system. Among the most serious complications of DM is diabetic retinopathy (DR), a condition driven by abnormal retinal neovascularization and dysregulated angiogenesis. These pathological changes increase vascular permeability, leading to retinal hemorrhage and, in severe cases, vision impairment or blindness (Wong *et al*, 2016; Duh *et al*, 2017). It is estimated that approximately 1 in 5 individuals with diabetes develop some degree of DR, with the incidence being particularly high in low- and middle-income countries where late diagnosis is common due to resource constraints. Early detection of DR is crucial, as timely intervention can prevent up to 95% of vision impairment and blindness. Current treatment strategies include laser therapy, vitrectomy, and anti-VEGF therapies (Wong *et al*, 2016; Duh *et al*, 2017). However, the prevalence of DR is rising rapidly, and there remains a significant unmet need for cost-effective, point-of-care diagnostic tools and targeted second-generation therapies to manage better and control the progression of this condition. Recent studies have shown that angiopoietin and *Tie* signaling plays a crucial role in protecting vascular dysfunction. During hyperglycemic conditions, the Ang-Tie signaling is severely affected (Saharinen *et al*, 2017).

Tie1 is a major effector protein during hyperglycemic conditions as it is a major player in neovascularization. Although its interactome and ligand remain a mystery, and it is often termed an orphan receptor (Mueller & Kontos, 2016; Sato *et al*, 1995). Recent investigations have shed light on their more complex involvement in regulating endothelial homeostasis and remodeling. *Tie1* in zebrafish and mice has been shown to affect endothelial cell angiogenesis and proper homeostasis *in vivo* (Carlantoni *et al*, 2021; Reinardy *et al*, 2015; D'Amico *et al*, 2010).

Moreover, functional studies indicate that *Tie1* plays a dual role in angiogenesis: it exerts a negative regulatory effect on *Tie2* levels within angiogenic tip cells, while positively regulating *Tie2* by forming heterodimers in stalk cells (Savant *et al*, 2015). These heterodimers are crucial for the maturation and remodeling of vessels through angiopoietin 1 signaling. Previous investigations suggested that Angiopoietin-1 binding independently to Tie2 and in heterodimeric association with *Tie1*, activating downstream signaling kinases such as PI3K/Akt pathway or Rho/Rac1, thereby modulating endothelial cell proliferation, migration, and survival(Saharinen *et al*, 2017; Joussen *et al*, 2021; Papapetropoulos *et al*, 2000; Saharinen *et al*, 2008). The regulation of *Tie1* and *Tie2* levels in vascular remodeling has been a focal point of research due to their potential as targeted therapies. Their involvement in diseases such as cancer metastasis and diabetic retinopathy underscores their clinical significance (Saharinen *et al*, 2017; Huang *et al*, 2010; Joussen *et al*, 2021; Augustin *et al*, 2009). It has prompted intensive investigation as they are the key player in angiogenesis and endothelial function.

Long noncoding RNAs (lncRNAs) are a significant and abundant class of regulatory molecules in endothelial cells, where they play a crucial role in controlling gene expression at various levels, including chromatin remodeling, transcription, and post-transcriptional processing. Recent discoveries, such as lncRNAs like *VEAL2, GATA-AS, SENCR, LASSI, STEEL, MANTIS, LEENE,* and *Tie1-AS*, have underscored their essential functions in regulating endothelial cell proliferation, migration, permeability, and stability. These lncRNAs have been extensively studied, revealing new mechanisms of action and interactions that continue to emerge. In addition to their regulatory roles, lncRNAs have shown promise as biomarkers for vascular diseases, given their high specificity, offering potential for early diagnosis and personalized treatment strategies. Given their pivotal role in vascular biology, lncRNAs are

121 increasingly recognized as both therapeutic targets and biomarkers for managing conditions like
122 diabetic retinopathy, where novel RNA-based interventions could provide significant clinical
123 benefits.

124 This study explores the RNA interactions of *Tie1*, a key protein involved in
125 neovascularization and complications in diabetic retinopathy (DR). Through a Tie1 pulldown
126 approach, we identified a previously uncharacterized and conserved lncRNA, *TAAL*, in human
127 endothelial cells and zebrafish. Our research highlights the critical role of lncRNA *TAAL* in
128 fundamental physiological processes such as tube formation and vascular permeability in
129 endothelial cells, with significant implications for vascular development in zebrafish embryos.
130 Notably, we discovered a crucial interaction between lncRNA *TAAL* and the *Tie1* protein, where
131 *TAAL* is essential for modulating *Tie1* protein stability. This relationship was further examined in
132 the context of DR, where lncRNA *TAAL* levels were notably upregulated in patient samples
133 compared to controls. These findings emphasize the importance of lncRNA *TAAL* in regulating
134 *Tie1*-mediated angiogenesis, permeability and vascular functions, particularly under diabetic
135 retinopathy conditions.

136 **Results**

137 **Protein-centric discovery of novel lncRNA - *Tie1*-associated angiogenic lncRNA**
138 **(*TAAL*)**

139 *Tie-1* plays a critical role in vascular development, as demonstrated in the mouse and zebrafish
140 models(Cao *et al*, 2023; Savant *et al*, 2015; Carlantoni *et al*, 2021). However, *Tie-1*'s interactome
141 and the molecular mechanisms regulating its expression remain poorly understood. Here, we
142 performed a protein-targeted pulldown of *Tie1* and determined if any *Tie1* protein-associated
143 long non-coding RNAs are involved in the angiogenesis pathway using HUVEC-hTert2 cell line.

144 We performed RNA immunoprecipitation (RIP) of *Tie1* protein followed by RNA-sequencing
145 (Figure 1A). After applying a stringent cutoff filter of greater than 5 fold change and -$\log_{10}$
146 (P-value) value greater than 2, we identified a bi-exonic polyadenylated lncRNA (Supply Fig
147 1A) and named it *TIE1-associated angiogenic lncRNA (TAAL) (previous names-*
148 *ENST00000457948.3, NONHSAG007003.2, RP11-79M19.2)(*Figure 1B). The lncRNA originates
149 from the intron between 2 and 3 exons of the GRK5 gene (Figure 1C). Further, it does not
150 exhibit any coding potential as computed using bioinformatic algorithms (Coding Potential
151 Assessment Tool (CPAT2) coding probability - 0.0003 (Wang *et al*, 2013); Coding Potential
152 Calculator (CPC2) coding probability - 0.0216282 (Kang *et al*, 2017))(Supply Fig 1B) . We also
153 performed ribosomal pulldown followed by RT-qPCR of the *TAAL* lncRNA and did not find any
154 ribosome enrichment on lncRNA *TAAL*, further suggesting it to be non-coding (Supply Fig 1C).
155 The second exon and promoter of lncRNA *TAAL* is observed to be conserved in mammals and
156 birds but is lost in reptiles and fish, exhibiting no sequence conservation. It also displays all the
157 epigenomic marks, including H3K27ac, H3K4me1, H3K4me3, and CAGE reads from ENCODE
158 data in HUVECs, suggesting it is a genuine transcript (Figure 1C) (ENCODE Project
159 Consortium *et al*, 2020). Expression profiling of the lncRNA using the GTEx v8 portal exhibited
160 it highly expressed in the testis, ovary, pituitary, lungs, and heart tissues (Supply Fig 2A)(Ferraro
161 *et al*, 2020). Next, we performed RIP-RT-qPCR to determine if the *TAAL* lncRNA also interacts
162 with *Tie2*. We did not find any enrichment of the lncRNA to the *Tie2* protein (Figure 1D).
163 Furthermore, to understand its localization, we performed subcellular fractionation and
164 qRT-PCR, which suggested that the *TAAL* lncRNA is cytoplasmic enriched (Figure 1E).
165 Single-molecule RNA *FISH* (*smFISH*) also demonstrates that *TAAL* lncRNA is enriched in the
166 cytoplasm (Supply Fig2B). We also performed co-immunofluorescent and *smFISH* for *TAAL*

lncRNA, *Tie1*, and *Tie2* proteins and observed colocalization of the lncRNA and proteins (Figure 1F). The interaction of *TAAL* lncRNA along with the *Tie1* protein suggests its *trans*-role in regulating protein function.

LncRNA *TAAL* modulates the pathophysiological functions of endothelial cells.

To understand the functionality of the lncRNA, we performed siRNA-mediated knockdown using siTAAL and overexpression using pcDNA3.1-TAAL plasmid. We observed significant knockdown and overexpression of the *TAAL* lncRNA transcript *in vivo* in the HUVEC-hTert2 cell line (Supply Fig 3 A-B). Next, we conducted scratch-wound assays and transwell migration assays to elucidate the migratory properties of cells upon lncRNA *TAAL* manipulation. Remarkably, the knockdown of lncRNA *TAAL* promoted enhanced wound closure and increased the migratory capacity of cells. In contrast, overexpression of lncRNA *TAAL* exerted a decrease in wound closure rate and an inhibitory effect on cell migration (Figure 2A-D). Additionally, BrdU proliferation assays corroborated our findings, demonstrating increased cell proliferation following lncRNA *TAAL* knockdown, while overexpression of lncRNA *TAAL* attenuated cellular proliferation (Figure 2E-F). Moreover, cell cycle analysis unveiled distinct alterations in cell cycle distribution patterns associated with lncRNA *TAAL* modulation. Specifically, the knockdown of lncRNA TAAL led to an accumulation of cells in the G0/G1 phase, indicative of an active proliferative state. In contrast, overexpression of lncRNA TAAL showed no significant change (Supply Fig I-J). Furthermore, we conducted a permeability assay using a collagen-coated transwell plate to assess the impact of lncRNA *TAAL* on cellular permeability. We observed a significant increase in permeability following the knockdown of lncRNA *TAAL*

189 (Figure 2G). Conversely, we noted a decrease in permeability upon the overexpression of
190 lncRNA *TAAL*, suggesting lncRNA's role in maintaining cellular barrier integrity (Figure 2H).
191 Next, we evaluated the angiogenic tube-forming function of the HUVEC-hTert2 cell under
192 knockdown and overexpression conditions. We observed that lncRNA *TAAL* knockdown cells
193 *(siTAAL)* were forming colonies but could not attain the tubular morphology on matrigel
194 compared to control transfection *(siControl)*. Similarly, upon *TAAL* lncRNA overexpression
195 (*pcDNA-TAAL*), we observed that cells could not attain the tubular morphology as seen in the
196 control pcDNA-3.1 transfection condition (Figure 2I-J). Next, we investigated cell viability's
197 potential influence on the perturbations in tubulogenesis observed upon manipulating lncRNA
198 *TAAL* expression levels. To comprehensively assess cell viability, we performed Annexin-V/PI
199 staining assays. We observed no significant change in cell viability following transfection with
200 siTAAL and pcDNA-*TAAL* constructs, suggesting the effects are not due to cellular toxicity but
201 rather the modulation of lncRNA *TAAL* expression (Figure 2K-L). These data together suggest
202 that lncRNA *TAAL* modulates the physiological function of endothelial cells.
203

204 **LncRNA *TAAL* regulates calcium-dependent cytoskeletal and junctional**
205 **dynamics.**

206 Given the observed alterations in proliferation and migration, we investigated the impact of
207 lncRNA *TAAL* modulation on cellular cytoskeletal dynamics. In the endothelial cells, we stained
208 the F-actin using Alexa Fluor 488 phalloidin to visualize cytoskeletal structures. Our analysis
209 revealed noteworthy changes in cytoskeletal organization upon knockdown and overexpression
210 of *TAAL* lncRNA. Specifically, *TAAL* lncRNA knockdown cells exhibited a marked increase in
211 the length and density of stress fibers, indicative of enhanced cytoskeletal stiffness (Figure 3A).

212 Furthermore, these cells elongated in cell length compared to their respective controls (Supply
213 Fig 5A). Conversely, overexpression of *TAAL* lncRNA elicited contrasting effects, with cells
214 displaying a reduction in both stress fiber length and cell size (Figure 3A). This suggests a role
215 for *TAAL* lncRNA in modulating cytoskeletal dynamics and cellular stiffness, potentially
216 influencing cellular morphology and migration ability.

217 Previous investigations have highlighted the involvement of endoplasmic reticulum (ER)
218 calcium dynamics in mediating cytoskeletal remodeling in endothelial cells (Shinde *et al*, 2013;
219 Tsai & Meyer, 2012; Tsai *et al*, 2014). Angiopoietin 1/2 mediated calcium regulation via the *Tie*
220 receptors has also been previously investigated and has been linked to angiogenesis (Pafumi *et*
221 *al*, 2015). Hence we investigated the impact of lncRNA *TAAL* modulation on intracellular
222 calcium levels, specifically focusing on calcium regulation within the ER. We assessed changes
223 in calcium dynamics by using live cell Ca^{2+} imaging with the ratiometric dye Fura2-AM.
224 Additionally, we employed the pharmacological inhibitor Thapsigargin (Tg) to deplete ER Ca^{2+}
225 stores, aiming to elucidate the role of *TAAL* in calcium homeostasis. Our observations revealed
226 significant alterations in calcium homeostasis upon manipulating lncRNA *TAAL* expression
227 levels. The knockdown of lncRNA *TAAL* resulted in a significant decrease in basal intracellular
228 calcium levels and a reduction in ER calcium content (Figure 3B-D). Conversely, overexpression
229 of lncRNA *TAAL* led to increased basal intracellular calcium levels and ER calcium content
230 (Figure 3E-G). Consistent with previous findings in cell culture and zebrafish models, which
231 have demonstrated that calcium spikes induce stress fiber contraction (Stolz & Bereiter-Hahn,
232 1988; Tiruppathi *et al*, 2002; Shinde *et al*, 2013; Dalal *et al*, 2020; Sahu *et al*, 2017), our results
233 suggest that changes in cytoskeletal dynamics associated with lncRNA *TAAL* modulation may be
234 mediated through alterations in calcium influx. We also checked the expression levels of a few

235 calcium modulator genes and observed that STIM1 levels were downregulated in *TAAL*
236 overexpressed cells (Supply Fig 6A-B). Also, upon modulation of lncRNA *TAAL*, the levels of
237 *STIM2* were significantly altered; in the knockdown state, it was suppressed, and in
238 overexpression of lncRNA, it was upregulated, correlating with the calcium levels inside the cell
239 upon similar conditions (Supply Fig 6C-D). We also observed decreased ORAI2 leaves upon
240 *TAAL* overexpression in the cells (Supply Fig 6 E-F). This suggests that intracellular calcium
241 dynamics, upon modulation of lncRNA *TAAL*, are governed by alterations in the levels of *STIM*
242 proteins,, a critical regulator of cellular and ER calcium homeostasis.

243 To further elucidate the underlying mechanisms contributing to changes in cellular
244 permeability following lncRNA *TAAL* alteration, we assessed mRNA levels of *VEGFR2* (KDR)
245 and VE-Cadherin (Hamdollah Zadeh *et al*, 2008; Phoenix *et al*, 2022; Bates & Curry, 1997;
246 Dalal *et al*, 2020; Gavard, 2013; Sandoval *et al*, 2001) but observed no significant changes
247 (Supplementary Fig 7A-D) . Next, we examined the localization of VE-Cadherin, an adhesion
248 protein regulated by the *Tie1-Tie2* signaling pathway and calcium influx. Our analysis revealed
249 that *TAAL* knockdown resulted in decreased membrane localization of VE-Cadherin, while *TAAL*
250 overexpression increased its membrane localization (Figure 3H). These findings collectively
251 suggest that modulation of lncRNA *TAAL* influences the VE-Cadherin membrane localization.

252

253 **_TAAL_ lncRNA is functionally conserved in zebrafish and modulates angiogenesis.**

254 To check if the lncRNA is functionally conserved across species, we performed a protein-centric
255 pulldown of *tie1* in zebrafish at 24 hpf, followed by RNA sequencing. Upon analysis, we
256 observed a lncRNA *ZFLNCG09997* (hereafter called lncRNA *taal*) was 4.7 fold enriched and
257 had a $-\log_{10}$ P-value greater than 15 (Figure 4A-B). The zebrafish *taal* lncRNA gene produces a 3

258 exonic polyadenylated lncRNA (Supply Fig 8A) with a transcript length of 2632bp observed on
259 chromosome 18 of zebrafish, arises antisense 5' upstream of endonuclease, polyU-specific C
260 (*endouc*). The *taal* lncRNA is noncoding in nature, as assessed through the online tool Coding
261 Potential Calculator (CPC2) (coding probability -0.0403034), and has no potential predicted
262 ORF. The *taal* lncRNA shows no sequence conservation with its human orthologue *TAAL*.

263 The expression profile analysis across adult tissues and developmental stages using
264 publicly available RNA seq data (Pauli *et al*, 2012; Yang *et al*, 2020; Sehgal *et al*, 2021)
265 unveiled the expression of the lncRNA in zebrafish's heart, testis, and skin (Figure 4C). We also
266 observed a prominent expression peak of the lncRNA *taal* during the bud stage, followed by
267 sustained expression at 48 hours post-fertilization (hpf) and 5 days post-fertilization (dpf) (Figure
268 4D). Intriguingly, an inverse expression pattern was observed for the protein-coding genes *tie1*
269 and *tie2* at 24 hpf, where their expression levels were markedly elevated while lncRNA *taal*
270 expression remained minimal. Notably, the initiation of angiogenesis from the posterior cardinal
271 vein (PCV) occurs during this developmental stage, implicating *tie1* and *tie2* in the sprouting and
272 angiogenesis process. The observed expression pattern of lncRNA *taal* suggests a potential
273 inhibitory role for *tie1* and *tie2* in angiogenesis during this critical developmental stage.

274 An antisense splice-blocking morpholino-based knockdown approach was employed to
275 elucidate further the functional significance of lncRNA *taal* in zebrafish development.
276 Knockdown of lncRNA *taal* resulted in notable defects in zebrafish angiogenesis, particularly
277 evident in patterning defects observed in the intersegmental vessels (ISVs) at 2 dpf (Figure 4E).
278 Additionally, investigation into the role of lncRNA *taal* in angiogenesis revealed enhanced
279 angiogenic sprouting from the subintestinal vessels (SIVs) in zebrafish injected with taal
280 morpholino near the SIV site as compared to control injections with scramble morpholino,

281 indicative of an anti-angiogenic role for lncRNA *taal*. Further confirmation of lncRNA *taal's*
282 functional conservation across species was attained through complementation and rescue assays.
283 Injection of a wild-type copy of human lncRNA *TAAL* demonstrated a reduction in angiogenic
284 sprouting when co-injected with *taal* morpholino, affirming the orthologous nature of lncRNA
285 *taal* between humans and zebrafish (Figure 4F). Moreover, an overexpression experiment of
286 lncRNA *TAAL* injected into the single-cell zebrafish embryos revealed abnormal vascular
287 patterning (Figure 4G). Furthermore, the injection of *TAAL* lncRNA at the SIV site led to a
288 reduction in the area of the SIV vessel formation (Figure H). This suggests a pivotal role of
289 zebrafish *taal* lncRNA in modulating angiogenic processes. These findings provide compelling
290 evidence that zebrafish *taal* lncRNA is a functional orthologue to human *TAAL* lncRNA and has
291 an important role in modulating and controlling angiogenic function in vertebrates.
292

293 **LncRNA *TAAL* negatively regulates *Tie1/2* protein turnover.**

294 To understand the molecular mechanism we examined the expression pattern of *Tie1* and *Tie2*
295 protein, with which the lncRNA *TAAL* interacts. We observed an increase in the protein
296 expression upon knockdown of the lncRNA *TAAL* and a decrease in the expression upon
297 overexpression of the lncRNA (Figure 5A). We also estimated *Tie1* and *Tie2* mRNA levels and
298 found no significant change in their mRNA expression upon knockdown and overexpression of
299 the lncRNA *TAAL* (Figure 5B). These findings indicate that lncRNA *TAAL* post-translationally
300 regulates the levels of *Tie1* and *Tie2* in endothelial cells. To further investigate this regulation, we
301 conducted immunofluorescence analysis of *Tie1* and *Tie2* under lncRNA *TAAL* knockdown and
302 overexpression conditions. In *TAAL* knockdown cells, we observed increased *Tie1* and *Tie2*
303 protein expression. Additionally, there was increased clustering of *Tie1* proteins and enhanced
304 colocalization of *Tie1* and *Tie2* within the cells. Conversely, overexpression of lncRNA *TAAL*

305 significantly reduced the *Tie1* and *Tie2* protein signals and decreased colocalization of *Tie1* and
306 *Tie2* (Figure 5C).
307

308 **LncRNA *TAAL* modulates *Tie1/2* protein turnover by ubiquitination.**

309 To elucidate the mechanisms underlying *Tie1/2* protein turnover, we employed proteomics using
310 LC/MS mass spectrometry on *TAAL* knockdown cells to identify the active pathways involved
311 (Figure 6A). Our gene ontology (GO) molecular function analysis revealed translation
312 dysregulation within cells upon knockdown of the lncRNA *TAAL*. Additionally, we observed the
313 upregulation of proteins with ubiquitin ligase inhibitor and ubiquitin-protein transferase inhibitor
314 activity (Figure 6B-C). To further validate our observation, we conducted a protein stability
315 assay using cycloheximide (10μM) treatment under conditions of both knockdown and
316 overexpression of lncRNA *TAAL*. Cycloheximide-mediated inhibition of translation resulted in
317 decreased stability of the *Tie1* protein in both knockdown and overexpression scenarios. This
318 indicates that the stability of *Tie1* is translation-dependent, with translation inhibition leading to
319 reduced *Tie1* stability (Figure 6D).

320 Previous studies have suggested that *Tie* protein degradation occurs via the proteasomal
321 pathway (Cheng & Hung, 2013; Wehrle *et al*, 2009) and as a receptor kinase, *Tie* may also be
322 degraded through the lysosomal pathway(Gu *et al*, 2022; Zhao *et al*, 2022; Kreitman *et al*, 2018).
323 To investigate this, we inhibited both the lysosomal and proteasomal pathways using the
324 pharmacological drug bafilomycin A1 (50nM) for lysosome and MG132(10μM) for proteasome
325 under conditions of knockdown and overexpression of lncRNA *TAAL*. Lysosomal pathway
326 inhibition enhanced *Tie1* protein stability, whereas proteasomal pathway inhibition compromised

327 stability and increased degradation (Figure 6E). These findings suggest that *Tie1* degradation
328 involves both pathways, with proteasomal inhibition leading to increased lysosomal degradation.
329 Next, we examined the ubiquitination patterns of *Tie1* and *Tie2* proteins as its associated
330 pathways were altered in proteomics studies. Knockdown of lncRNA *TAAL* resulted in increased
331 ubiquitination of *Tie1* and decreased ubiquitination of *Tie2*. Conversely, overexpression of
332 lncRNA *TAAL* led to decreased ubiquitination of *Tie1* and increased ubiquitination of *Tie2*
333 (Figure 6F). These findings and insights from previous literature suggest that lncRNA *TAAL* may
334 mediate the recruitment of specific ubiquitin ligases to *Tie1*, facilitating its ubiquitin-mediated
335 lysosomal degradation. In the absence of lncRNA *TAAL*, the recruitment of appropriate ubiquitin
336 ligases is impaired. Alternatively, we hypothesize that in the absence of *TAAL,* there could be the
337 formation of heterotypic chains of ubiquitin on *Tie1* protein, leading to the binding of other
338 ubiquitin-like proteins and thereby enhancing its stability (Figure 6G). Furthermore, the
339 upregulation of ubiquitin ligase inhibitors under *TAAL* knockdown conditions significantly
340 modulates the ubiquitin-degradation system, which is essential for the targeted degradation of
341 *Tie1* proteins. The stability of both *Tie1* and *Tie2* proteins is enhanced by inhibiting ubiquitin
342 ligases. These observations indicate that lncRNA *TAAL* plays a crucial role in regulating the
343 ubiquitin-mediated lysosomal degradation of *Tie1/2*, thereby controlling protein turnover.
344

345 **lncRNA *TAAL* is negatively regulated in diabetic retinopathy.**

346 To investigate the disease association of lncRNA *TAAL*, we focused on retinopathy, a progressive
347 neovascularization condition often resulting from diabetes. *Tie1/2* signaling pathway has been
348 shown to play an important role in neovascularization during diabetic conditions. Hence we
349 analyzed the expression of lncRNA *TAAL* in endothelial cells under hyperglycemic conditions.

High glucose treatments (25 mM and 50 mM) significantly downregulated lncRNA *TAAL* expression (Figure 7A). Data from the Noncode database revealed that lncRNA *TAAL* is present in extracellular vesicles secreted by HUVEC cells (Figure 7B) (Fang *et al*, 2018). Next, to validate our observation we examined the lncRNA *TAAL* expression in diabetic patients at various stages of retinopathy including patients having diabetes mellitus with no retinopathy (n=50), non-proliferative diabetic retinopathy (NPDR)(n=70), and proliferative diabetic retinopathy (PDR)(n=50) and compared it to control (n=60). We observed a significant enrichment of lncRNA *TAAL* in the blood samples of of NPDR (FC- 2.92; p-value < 0.001) and PDR (FC- 4.107; p-value < 0.001) patients compared to controls and other diabetic conditions (FC- 1.121; p-value - ns) (Figure 7C). Additionally, upon categorizing retinopathy based on its severity we observed that lncRNA TAAL was significantly higher in case of mild NPDR (FC 2.15, *p*-value <0.05), moderate NPDR (FC 3.99, *p*-value <0.001), severe NPDR (FC 2.66, *p*-value <0.05) and PDR (FC 4.1, *p*-value <0.00001) as compared to the healthy controls (Supply Fig 9A-B). Using normalized Ct values from NPDR patients versus controls, ROC curve analysis showed a significant correlation between NPDR and PDR with the lncRNA *TAAL* expression. We also computed the ROC area under the curve and observed a significant specificity and sensitivity for both NPDR (AUC- 0.6763; p-value - 0.004) and PDR (AUC- 0.7649; p-value < 0.0001) compared to control group (Figure 7 D-E). We next modeled the hyperglycemic conditions in HUVEC-hTert2 cells to mimic diabetic retinopathy and to understand the permeability defect associated with this condition. Hyperglycemic condition significantly increased FITC-dextran permeability across the endothelial monolayer (Figure 7F). We also observed decreased surface localization of VE-cadherin, a key adhesion molecule, under hyperglycemic conditions (Figure 7G). Next, we investigated the potential of lncRNA *TAAL* to

modulate endothelial permeability. Overexpression of lncRNA *TAAL* significantly reduced permeability and restored VE-cadherin localization to the membrane under hyperglycemic conditions, as it decrease the *Tie1/2* levels inside the cells..

To investigate the transcriptional regulation and impact of complementation on *TAAL* lncRNA under hyperglycemic conditions, we employed a luciferase reporter assay. This approach allowed us to determine whether the expression of lncRNA *TAAL* is regulated via a positive feedback loop upon complementation in hyperglycemia condition. We cloned the lncRNA *TAAL* promoter into the psiCHECK2 plasmid upstream of Renilla luciferase and performed assays in normal and hyperglycemic conditions. Hyperglycemia significantly decreased luciferase activity, suggesting high glucose inhibits lncRNA *TAAL* transcription. Furthermore, overexpression of lncRNA *TAAL* restored its transcription, indicating a positive feedback loop modulating its own expression. These data collectively underscore the significant role of lncRNA *TAAL* in modulating pathological conditions associated with diabetic retinopathy. We hypothesize that under hyperglycemic conditions, the transcription of lncRNA *TAAL* is downregulated by inhibiting its transcription. This process creates an environment that increases *Tie1* stability and promotes neovascularization, leading to pathological diabetic retinopathy. lncRNA *TAAL* has potential as a biomarker for predicting the progression from normal diabetes to diabetic retinopathy, as it is released into the bloodstream during retinopathy and can be detected by qRT-PCR. Furthermore, lncRNA *TAAL* exhibits high therapeutic potential for restoring normal conditions under hyperglycemia.

Discussion

In this study, we utilized a protein-centric approach to identify interacting partners of the major endothelial receptor protein *Tie1* in HUVEC-hTert2 cells. We identified a novel, uncharacterized

397 lncRNA named *TAAL*, whose modulation influences vascular function and integrity. Further
398 investigations revealed that lncRNA *TAAL* modulates cellular calcium dynamics, affects
399 cytoskeletal movements, and regulates VE-cadherin localization at cell junctions(Figure 3).
400 Molecular analyses provided evidence that lncRNA *TAAL* controls the protein turnover of *Tie1*
401 through the regulation of ubiquitin-mediated degradation and stability. Moreover, we identified a
402 functional orthologue of human lncRNA *TAAL* in zebrafish, which does not exhibit any sequence
403 conservation but has a common interacting partner *Tie1*. Knockdown of zebrafish *taal* resulted
404 in angiogenic defects in the ISVs and SIVs (Figure 4 E-H). Rescue experiments demonstrated
405 that human lncRNA *TAAL* can complement the function of zebrafish lncRNA *taal*, suggesting
406 evolutionary conservation of function (Figure 4F). Our findings propose a negative regulatory
407 role of *TAAL* over *Tie1,* thereby modulating its protein turnover. We further investigated the role
408 of lncRNA *TAAL* in diabetic retinopathy a neovascular eye disease. We observed that the
409 expression of lncRNA *TAAL* was significantly upregulated in patients with NPDR and PDR
410 conditions (Figure 7C). Overexpression of lncRNA *TAAL* in a hyperglycemic model of HUVEC
411 cells decreased permeability defects by restoring VE-cadherin at the membrane (Figure 7F-G).
412 Additionally, overexpression of lncRNA *TAAL* induced a positive feedback loop, which enhanced
413 the transcription of endogenous lncRNA *TAAL* (Figure 7H). Our investigation suggests that
414 lncRNA *TAAL* is an important regulator of *Tie1* protein turnover and could be an effective
415 therapeutic target for neovascular eye diseases.

416 Angiopoietin-Tie signaling is a crucial pathway for targeting various cancers and vascular
417 eye diseases, specifically diabetic retinopathy (Saharinen *et al*, 2017; Joussen *et al*, 2021;
418 Huang *et al*, 2010). *Tie1*, an orphan receptor, has been identified as an interacting receptor for
419 angiopoietin-1 in a heterodimeric form with *Tie2*. In endothelial cells, the dynamics of *Tie1* and
420 *Tie2* interaction and modulation play a significant role in their function. *Tie1* is a major protein
421 associated with the angiogenic function of endothelial cells, particularly when *Tie2* levels are
422 minimal. In the quiescent state, Tie2 levels are upregulated to maintain the survival of

423 endothelial cells, while Tie1 levels remain low. During vascular remodeling, stalk cells exhibit a
424 balance of Tie1 and Tie2 levels, underscoring the importance of both proteins (Savant *et al*,
425 2015). Modulating the interaction and levels of Tie1 and Tie2 *in vivo* holds promise for regulating
426 endothelial cell functions. Inhibition of Angiopoietin-1 has been an effective strategy to modulate
427 Tie1 levels and function during angiogenesis and disease conditions. Additionally, recent
428 findings have identified *LECT2* as a receptor for *Tie1*, showing promising results in controlling
429 angiogenesis and liver fibrosis in vivo (Xu *et al*, 2019). The development of second-generation
430 targeted therapies for *Tie1* using antibodies has also demonstrated encouraging results in
431 preclinical animal models, controlling angiogenesis and metastasis in cancer (Singhal *et al*,
432 2020; La Porta *et al*, 2018). With advancements in RNA modification and the emergence of
433 RNA-based targeted therapies(Sparmann & Vogel, 2023; Saw & Song, 2024; Zhu *et al*, 2022) ,
434 targeting a modulator of *Tie1* protein presents an intriguing approach. Our findings provide
435 evidence that lncRNA *TAAL* can effectively modulate *Tie1* levels *in-vivo,* inhibiting downstream
436 functions to control vascular remodeling. *TAAL* lncRNA serves as a promising candidate for
437 RNA-based target therapy for modulating *Tie1* levels and its associated pathways in vascular
438 diseases such as diabetic retinopathy and cancer metastasis.

439 LncRNAs have been shown to perform myriad functions within cells, primarily
440 determined by their localization to the nucleus, chromatin, or cytoplasm. Cytoplasmic lncRNAs
441 are of particular interest due to their accessibility for therapeutic targeting in various disease
442 conditions. In the cytoplasm, lncRNAs are known to interact with proteins and regulate their
443 functions and translation. Several studies, including those on lncRNAs such as *VEAL2,*
444 *CamK-A, LINK-A, RP11-624L4.1, ECRAR, AGPG, and MetaLnc9 (LINC00963)*, have
445 demonstrated that lncRNAs can interact with kinase proteins and modulate their signaling
446 (Sehgal *et al*, 2021; Sang *et al*, 2018; Lin *et al*, 2016; Zhou *et al*, 2020; Chen *et al*, 2019; Liu *et*
447 *al*, 2020; Yu *et al*, 2017). These interactions suggest roles for lncRNAs in acting as
448 substrate-binding competitors, controlling localization, translation, and stability of kinase

449 proteins. In our investigation, we found that the lncRNA *TAAL* controls the turnover of the
450 receptor kinase *Tie1* protein. We hypothesize that in the absence of *TAAL* lncRNA, *Tie1*
451 undergoes poly-ubiquitination with heterotypic chains of either K6 or K11 linkage, which are
452 known to stabilize the protein (Tracz & Bialek, 2021; Hong *et al*, 2018; Abu Ahmad *et al*, 2021).
453 These K6 and K11 chains of ubiquitin are known to evade lysosomal-mediated degradation by
454 binding with ubiquitin-like proteins, thereby stabilizing the protein. Under normal conditions,
455 poly-ubiquitination with either K63 or K48 linkage homotypic chains is associated with lysosomal
456 degradation (Hong *et al*, 2018). The lncRNA *TAAL* may facilitate proper ubiquitination by
457 recruiting E3 ligase to the *Tie1* protein. In hyperglycemic conditions, there is a complete
458 shutdown of *TAAL* production in endothelial cells, and the remaining *TAAL* is removed via
459 exocytosis. The absence of *TAAL* leads to poly-ubiquitination with heterotypic chains at the *Tie1*
460 kinase domain, where ubiquitin-like proteins attach to these chains and protect them from
461 degradation. Understanding the targets involved in proper ubiquitination of *Tie1* and the
462 ubiquitin-like proteins that protect *Tie1* from degradation warrants further investigations. The
463 protection of *Tie1 from degradation leads* to activation of *Tie1* downstream signaling cascades.
464 This in turn results in change in cytoskeleton dynamics due to dysregulation of calcium
465 dynamics, and alteration in localization of VE-cadherin on the surface of the cells (Figure 8). In
466 this study we provide a detailed assessment and molecular function of lncRNA *TAAL* in vascular
467 remodeling. Going forward, a comprehensive investigation is required to elucidate further the
468 ubiquitination machinery involved in regulating *Tie1* expression.

469 Protein-centric targeted approaches in identifying lncRNA interactomes have shown
470 great promise in selecting lncRNA modulators of disease-associated protein targets. These
471 approaches are valuable not only for identifying orthologous lncRNAs across species that lack
472 sequence conservation but also for understanding the multifaceted roles of lncRNAs in various
473 biological processes(Ranjan *et al*, 2021; Diederichs, 2014; Ulitsky, 2016). Our recent work
474 demonstrated that lncRNA *veal2* which was identified in zebrafish, has shown its interaction with

475 *prkcb2*. A protein-centric pulldown technique was utilized to identify the human ortholog for
476 zebrafish *veal2* without sequence conservation. *VEAL2* was shown to be a promising target and
477 biomarker for proliferative diabetic retinopathy (PDR) patients, regulating vascular permeability
478 (Sehgal *et al*, 2021). Similarly, lncRNA *JPX* a modulator of *XIST* lncRNA, which interacts with
479 the *CTCF* protein, highlighted that this interaction is a conserved function of lncRNA *JPX*
480 despite the absence of sequence conservation between human and mouse ortholog (Karner *et*
481 *al*, 2020). In this study, we observed that despite the lack of sequence conservation between
482 human and zebrafish lncRNA *TAAL*, *Tie1* is a conserved interacting partner, and *TAAL* functions
483 similarly in both species. The conservation of lncRNA functions across species, even in the
484 absence of sequence conservation, underscores the importance of considering alternative
485 modes of conservation. Conservation based on motif or syntenic conservation has only
486 identified a small proportion of orthologues and a large number of lncRNA remains unknown for
487 their mode of conservation. Since many lncRNAs show little to no sequence conservation,
488 focusing on protein-centric interactions can fill critical gaps in our understanding of lncRNA
489 conservation and function. This targeted protein-centric approach can effectively identify
490 functional conserved orthologous lncRNAs, providing insights into their evolutionary significance
491 and biological roles.

492 In summary, we have identified a novel and uncharacterized lncRNA, *TAAL*, using a
493 protein-centric pulldown approach. LncRNA *TAAL* plays a significant role in endothelial cell
494 migration, permeability, and angiogenesis. By using *Tie1* as bait, we also identified the zebrafish
495 ortholog of *TAAL*. Knockdown of zebrafish *taal* resulted in angiogenic defects in the
496 intersegmental vessels (ISV) and subintestinal vessels (SIV), which were successfully rescued
497 by human *TAAL*. Molecular investigations revealed that lncRNA *TAAL* regulates *Tie1* protein
498 turnover by modulating its ubiquitination and subsequent degradation. Additionally, we observed
499 that lncRNA *TAAL* levels were significantly upregulated in patients with diabetic retinopathy
500 (NPDR & PDR), indicating its potential clinical relevance. Overexpression of lncRNA *TAAL* in

501 hyperglycemic conditions restored endothelial cell permeability defects by enhancing the
502 recruitment of VE-cadherin to membrane junctions. Our findings suggest that lncRNA *TAAL*
503 plays a crucial role in regulating *Tie1* stability and function, highlighting its potential as a
504 therapeutic target for vascular eye diseases.

505 **Structured Methods - Reagents and Tools Table**

Reagent/Resource	**Reference or Source**	**Identifier or Catalog Number**
Experimental Models		
gib004Tg(fli1a:EGFP; *gata1a*:DsRed) (*Danio rerio*)	Sridhar Sivasubbu lab, CSIR-IGIB,(Lalwani *et al*, 2012; Lawson & Weinstein, 2002; Traver *et al*, 2003)	*gib004Tg(fli1a*:EGFP; *gata1a*:DsRed)
HUVEC-hTERT2	ATCC	CRL-4053
Recombinant DNA		
pcDNA3.1+	Thermo scientific	V79020
pcDNA-TAAL	This study	Gene script
HA-Ubiqutin plasmid	Addgene	18712
psi-CHEK-2	Promega	C8021
Antibodies		
Tie1	Thermo scientific	PA5-32618
IgG	Abcam	ab231712
Tie2	Cell Signaling Technology	23111S
Tie1	Cell Signaling Technology	4224S
GAPDH	Cell Signaling Technology	2118S
VE-Cadharine	Abcam	ab33168
Alexa Fluor™ 488	Thermo scientific	
Alexa Fluor™ 647	Thermo scientific	
HA antibody	Cell Signaling Technology	3724
Annexin V-FITC	Thermo scientific	A13201
Anti-rabbit IgG, HRP-linked Antibody	Cell Signaling Technology	7074S

Oligonucleotides and other sequence-based reagents		
PCR primers	This Study	Eurofins
taal Morpholino	This study	Gene tools
Scrambled MO	Vivo-Morpholino Standard Control Oligo-Gene tools	Gene tools
Stellaris RNA FISH	This study	LGC Biosearch Technologies
siRNA	Dharmacon	Supply Table
siTAAL	This study	Supply Table
Chemicals, Enzymes and other reagents		
Lipofectamine 3000	Invitrogen	L3000015
Yeast tRNA	Thermo scientific	AM7119
BSA	Sigma	A9418
Vascular Cell Basal Medium	ATCC	PCS-100-030
Endothelial Cell Growth Kit-BBE	ATCC	PCS-100-040
Pierce™ Protein A/G magnetic beads	Thermo Scientific	88803
Proteinase K	HiMedia	
Dual-luciferase reporter assay kit	Promega	E1910
TRIzol	Invitrogen	15596026
N- phenylthiourea	Sigma Aldrich	P7629
T7 mMESSAGE mMACHINE kit	Thermo Scientific	AM1344
3-aminobenzoic acid (Tricaine)	Sigma Aldrich	E10521
TB Green Premix Ex Taq II (Tli RNase H Plus)	Takara	RR82LR
TruSeq RiboPlus RNA Preparation Kit	Illumina	

ProLong™ Gold Antifade Mountant with DNA Stain DAPI	Thermo Scientific	P36941
Corning® Matrigel® Basement Membrane Matrix, *LDEV-Free	Corning	354234
Propidium Iodide	Sigma Aldrich	P4170
Paraformaldehyde	Sigma Aldrich	158127
RNase	Sigma Aldrich	R6148
Fluorescein isothiocyanate–dextran	Sigma Aldrich	46945
Fura-2 AM	Thermo Scientific	F1221
Protease inhibitor cocktail	Roche	04693159001
DyNAmo ColorFlash SYBR Green qPCR Kit	Thermo scientific	F416L
Formaldehyde	Sigma Aldrich	F8775
RIPA lysis buffer	Thermo scientific	89900
Verso cDNA Synthesis Kit	Thermo scientific	AB1453A
SSRT II	Thermo scientific	18064022
Alexa Fluor 488 phalloidin	Thermo scientific	A12379
Sequencing Grade Modified Trypsin	Promega	V5111
Immobilon Forte Western HRP substrate	Sigma Aldrich	WBLUF0500
Software		
Zfin	https://zfin.org/	
STAR v2.7	https://github.com/alexdobin/STAR	
Coding Potential Assessment Tool	http://lilab.research.bcm.edu/	
Coding Potential Calculator	https://cpc.gao-lab.org/	
DESeq2.	https://github.com/thelovelab/DESeq2	

PeakView® software	Sciex	
MarkerView® software	Sciex	
htseq-count	https://github.com/simon-anders/htseq	
GraphPad Prism v9	Graph Pad	
ImageJ FIJI	https://github.com/fiji/fiji	
FlowJo software 10	BD	
Other		
Novaseq 6000	illumina	
Harvard Apparatus pump	Harvard Apparatus	
Stereo microscope Zeiss	ZEISS	
LightCycler LC480	Roche	
CFX384 BioRad	BioRad	
Zeiss Axioscope A1 fluorescent microscope	Carl Zeiss	
Infinite® Lumi plate reader	TECAN	
Zeiense confola mirosoe	Carl Zeiss	
Nikon Eclipse Ti2 microscope	Nikon	
TripleTOF 6600	Thermo scientific	
BD FACSVerse Cell Analyzer	BD	
EVOS	Thermo scientific	

Materials and Method

Ethical approvals

Zebrafish used in this study is a double transgenic zebrafish (*Danio rerio*) *gib004Tg(fli1a*:EGFP; *gata1a*:DsRed) (Lalwani *et al*, 2012; Lawson & Weinstein, 2002; Traver *et al*, 2003). The zebrafish were cared for and maintained in-house following standard operating

512 procedures approved by the Animal Ethics Committee of CSIR-Institute of Genomics and
513 Integrative Biology, India (GENCODE-C-24). Special care was taken to ensure minimal distress
514 to the animals.

515 The human study participants were recruited from Smt. Kannuri Santhamma Centre for
516 vitreoretinal Diseases, L V Prasad Eye Institute, Hyderabad, India. The study was done
517 according to the guidelines of Declaration of Helsinki and study was approved by Institutional
518 Review Board (LEC-BHR-P-04-21-626).

519 **Cell line**

520 We used Human umbilical vein endothelial cell lines HUVEC-hTert2 cell line (CRL-4053,
521 ATCC) for our experiments (Karner *et al*, 2020; Takano *et al*, 2008). The cells were grown in
522 Vascular Cell Basal Medium (PCS-100-030, ATCC) supplemented with Endothelial Cell Growth
523 Kit-BBE (PCS-100-040, ATCC) incubated at 37 C with 5% CO2.

524 **RNA-Immunoprecipitation and RNA-sequencing**

525 For RNA immunoprecipitation, we used ~8 million HUVEC-hTert2 cells from two T75 flasks,
526 and 500 zebrafish embryos at 24 hpf. UV cross-linking was performed according to a previously
527 described protocol. Cell and zebrafish lysates were prepared using RIPA buffer supplemented
528 with protease inhibitors. The cell lysate was incubated with protein A/G beads for pre-clearing
529 for 2 hours at 4°C. Fresh protein A/G beads were blocked using 1x BSA and yeast tRNA for 1
530 hour at room temperature. The cell lysate, protein A/G beads, and the 1ug of primary antibody of
531 *Tie1* (Thermo - PA5-32618) or *Tie2* (CST-23111S) were mixed together and incubated overnight
532 on an orbital rotor at 4°C. The beads were then pulled down and washed with RIPA buffer. The
533 beads were subsequently incubated in PNK buffer with proteinase K at 55°C for 45 minutes.
534 Following incubation, the beads were dissolved in TRIzol, and RNA was isolated using the
535 phenol-chloroform method. The isolated RNA was used for first-strand cDNA preparation using

536 SSRT-II. The RNA-seq library was prepared using the TruSeq RiboPlus RNA Preparation Kit
537 according to the manufacturer's instructions. Finally, the library was sequenced on a NovaSeq
538 6000 platform.

539 The reads were aligned as previously described using STAR aligner to human reference genome
540 hg38 and zebrafish reference genome Zv9 and reads were count using htseq -count function
541 (Dobin *et al*, 2013; Anders *et al*, 2015; Ranjan *et al*, 2024).

542 **Western blot**

543 Cells were lysed using NP40 lysis buffer supplemented with protease inhibitors and quantified
544 using a BCA kit. The lysate was run on a 10% SDS-PAGE gel and transferred to a PVDF
545 membrane. Primary antibodies for *Tie1* (CST-4224S) and *Tie2* (CST-23111S) were diluted to a
546 concentration of 1:1000 and incubated overnight at 4°C. Secondary HRP-conjugated antibodies
547 at 1:10000 dilution were incubated for 1 hour at room temperature. Immunoblotting was
548 visualized using ECL under a chemiluminescence gel documentation system.

549 **Single molecular FISH and Immunofluorescent**

550 We performed smFISH as per the manufacturer's protocol (Biosearch Technologies). Both
551 smFISH and co-immunofluorescence were conducted according to the provided instructions.
552 Briefly, cells were grown on coverslips and fixed in 1% formaldehyde for 10 minutes, followed
553 by three washes with 1X PBS. The cells were then permeabilized using 70% ethanol overnight at
554 4°C. After washing with 1X PBS three times, the cells were incubated in Buffer A for 10
555 minutes. The coverslips were then incubated with a hybridization buffer containing smFISH
556 probes for *TAAL* lncRNA and primary antibody at a 1:200 dilution in a humidified chamber for
557 16 hours at 37°C. Following hybridization, the cells were washed with Wash Buffer A and
558 incubated with a secondary antibody conjugated with Alexa Fluor for 30 minutes in the dark.

559 The cells were subsequently washed with Wash Buffer B, mounted on slides using Anti-fade
560 Gold mounting media with DAPI, and fixed. Confocal imaging of the fixed slides was performed
561 at 63X magnification with oil immersion. The data were processed and deconvolution was
562 performed using FIJI ImageJ software and its plugins (Schindelin *et al*, 2012).

563 **Subcellular fraction**

564 The subcellular fractionation of HUVEC-hTert2 was carried out following a modified version of
565 the protocol described (Ten *et al*, 2012). In brief, T25 flask of HUVEC-hTert2 cells were
566 incubated and homogenized in a hypotonic buffer consisting of 10 mM HEPES (pH 7.9), 1.5
567 mM $MgCl_2$, 10 mM KCl, 0.5 mM DTT, and a protease inhibitor. This mixture was then
568 centrifuged at 1000 rpm for 5 minutes at 4°C. The supernatant, containing the cytoplasmic
569 fraction, was separated, while the pellet, containing the nuclear fraction, was washed with the
570 hypotonic buffer and collected. A small portion (1%) of each sample was set aside for western
571 blot analysis, and the remainder was used for RNA extraction.

572 **Tube formation assay**

573 Tube formation assay was performed on matrigel as previously described (Chatterjee *et al*,
574 2024). Briefly, the knockdown and overexpression of lncRNA TAAL in HUVEC-htert2 cells
575 were taken for the assay. Matrigel was thawed and prepared as per the manufacturer's protocol
576 and was coated in a 48-well plate. 40,000 cells were taken for the assay from each condition and
577 was loaded on top of the solidified matrigel with complete HUVEC mediate. The cells were
578 incubated for 4-5 hrs at 37 °C and 5% CO2 and tube formation was imaged in EVOS or Nikkon
579 microscope.

580 **Scratch wound assay**

581 Scratch wound assay was performed as previously described (Sehgal *et al*, 2021). Briefly,
582 HUVEC-hTert2 cells were transfected with siRNA and pcDNA3.1 plasmid targeting TAAL
583 lncRNA for its knockdown and overexpression. Cells were grown in 24 well plates till the
584 monolayer was formed, and before the experiment, the cells were incubated in HUVEC media
585 without FBS. Using the p200 tip a scratch was made in the well, the media and cell debris were
586 washed using 1 X PBS and incubated in HUVEC media with FBS for 24 hrs, and imaging was
587 done in EVOS or Nikkon microscope.

588 **Annexin -V assay**

589 Cell apoptosis was detected using an Annexin/PI-based assay. The HUVEC-htert2 cells were
590 harvested after transient knockdown and overexpression of TAAL for 48 hours and resuspended
591 in an annexin binding buffer. To this, Annexin V-FITC and Propidium Iodide (PI) were added in
592 the dark for 10 min. Then, the data was acquired using BD FACSVerse Cell Analyzer (BD
593 Bioscience) and the results were analyzed using FlowJo software 10.

594 **Cell cycle assay**

595 To assess cell cycle progression upon knockdown and overexpression of *TAAL*, HUVEC-hTert2
596 cells were seeded in a 6-well plate. After 48 hours, cells were harvested and kept in 70% ethanol
597 for 24 hours at -20 0 C. The next day, cells were treated with RNase at 37 0 C for 1 hour, then
598 stained with Propidium Iodide (PI) in the dark for 30 minutes. The cell cycle distribution was
599 detected using BD FACSVerse Cell Analyzer (BD Bioscience).

600 **Permeability assay**

601 Permeability assay was performed as previously described (Sehgal *et al*, 2021). Briefly, lncRNA
602 TAAL knockdown and overexpressed cells, along with control, were taken for the experiment. 1
603 million cells were seeded on the collagen-coated membrane's upper chamber and incubated until

604 the monolayer is formed. After the monolayer is formed, the media from the upper chamber is
605 removed and supplemented with fresh media with fluorescein isothiocyanate (FITC) conjugated
606 dextran (Sigma, USA) at 1mg/ml final concentration. The sample was incubated and after every
607 30 min, the media from the lower chamber was collected for 3 hours. UV spectrometer reading
608 was taken on a monocular reader, and the FITC-dextrans efflux percentage was calculated.

609 **Ubiquitin assay**

610 The ubiquitin pulldown was performed as previously described (Li *et al*, 2023). Briefly,
611 HUVEC-hTert2 cells were cotransfected with siRNA / overexpression plasmid of TAAL
612 lncRNA with HA-Ubiqutin plasmid (Addgene# 18712). The cells, after 48 hrs of treatment, were
613 treated with MG132 for 8 hours and then harvested. The cells were washed with 1xPBS, and cell
614 lysate was prepared using RIPA buffer (Thermo Scientific) having protease inhibitor and
615 iodoacetamide. Cell lysate was precleared using protein A/G beads, and the primary antibody of
616 target Tie1, and Tie2 was incubated with fresh protein A/G beads separately at room temperature
617 for 2 hr. The cell lysate, proteinA/G bead conjugated primary antibody, was incubated overnight
618 at 4 °C on the orbital rotor. ProteinA/G beads were pulled down and washed 3 times with RIPA
619 buffer. The beads were dissolved in an SDS loading buffer and heated at 95 °C for 10 min. The
620 sample was run on 10% SDS PAGE gel and was transferred on PVDF membrane. The blot was
621 probed with HA antibody at 1:2000 dilution overnight at 4°C and the secondary was incubated at
622 room temperature for 1 hr. Immunoblotting was visualized using ECL under a
623 chemiluminescence gel documentation system.

624 **Morpholino designing and zebrafish microinjection**

625 Antisense morpholino oligonucleotide (MO) was designed to target the exons -intron boundaries
626 of the lncRNA *taal*. The MO was ordered from GeneTools, redissolved in 300 ul to make 1mM

627 stock, and stored in -20 °C for further use. We used 100uM concentration of each MO targeting
628 both the introns and co-injected it into single-cell zebrafish or 2dpf zebrafish at SIV using
629 FemtoJet injection system and Nikkon microscope. After injection, the embryos were transferred
630 to (0.003%) PTU (N- phenylthiourea, Sigma Aldrich) water and further incubated at 28°C. Water
631 was changed every 24 hrs, and dead embryos were discarded. Human lncRNA TAAL was
632 amplified and converted into RNA using Invitro transcription kit T7mMassage mMachine
633 (Thermo scientific). We injected 100ng/ul concentration into single-cell zebrafish or 2dpf
634 zebrafish at SIV as described previously (Habeck *et al*, 2002; Sehgal *et al*, 2021).

635 **RT-qPCR**

636 RNA isolation was done using TRIzol and phenol chloroform method and the samples were
637 DNAses treated. RNA was converted to cDNA using an SSRTII (Thermo scientific) enzyme as
638 instructed by the manufacturer. RT-qPCR was perfomred for taregt gene using TB Green SyBr
639 (Takara) on Biorad CFX96 machine. The data was analyzed as described previously (Winer et
640 al., 1999; Livak and Schmittgen, 2001).

641 **Proteomics**

642 After knockdown using siRNA TAAL and siControl, cells were lysed using RIPA -lysis buffer.
643 Proteins were precipitated with acetone chilled at -20°C. Supernatants were transferred, and four
644 volumes of chilled acetone were added to it. After vortexing and incubation at -20°C for
645 overnight, samples were centrifuged at 10,000 × g for 15 minutes at 4°C. The supernatant was
646 discarded, the pellet air-dried, and resuspended in base buffer (Tris-Cl pH 8 (50 mM)). Protein
647 concentration was determined by BCA assay. This sample was subjected to trypsin digestion
648 (sequencing grade, Promega). 20ug of protein in 20 µl of base buffer was reduced with 2 µl of 25
649 mM DTT at 56°C for 30 minutes, followed by alkylation with 1 µl of 55 mM iodoacetamide at

650 room temperature in the dark for 15 minutes. After adding 2 µl of trypsin (1 µg/µl), samples
651 were incubated at 37°C for 18 hours. Digestion was terminated with 0.5% formic acid, and
652 samples were vacuum evaporated at 30°C.

653 The peptides were fractioned into 8 fractions using a strong cation exchange column- ICAT (AB
654 Sciex). Ellution of the peptide was done with a gradient concentration of ammonium formate
655 buffer. The fractionated peptides were analyzed using a quadrupole-TOF hybrid mass
656 spectrometer (TripleTOF 6600, AB Sciex, USA) coupled with a nano-LC system (Eksigent
657 NanoLC-425) in SWATH mode for relative quantitation. Desalted peptides (5 µg) were initially
658 loaded onto a trap-column (ChromXP C18CL 5 µm 120 Å, Eksigent) for additional desalting.
659 Separation was performed on a reverse-phase C18 analytical column (ChromXP C18, 3 µm 120
660 Å, Eksigent) at a flow rate of 5 µl/minute with buffer A (water containing 0.1% formic acid) and
661 buffer B (acetonitrile containing 0.1% formic acid). Each sample had a runtime of 50 minutes,
662 followed by a 10-minute equilibration period before the next run. The raw data files generated by
663 the instrument were imported into PeakView® software for further analysis. The prepared
664 HUVEC-htert2 proteome ion library was utilized to identify MS/MS peaks, while relative
665 quantitation of different proteins was conducted using MarkerView® software (AB Sciex).

666 **Luciferase assay**

667 The promoter of lncRNA *TAAL* was cloned into the psiCHECK-2 plasmid using *NheI* and *KpnI*
668 restriction enzymes, positioned in front of the renilla luciferase gene. HUVEC-hTert2 cells were
669 transfected with siRNA and an overexpression plasmid for lncRNA *TAAL* along with
670 psiCHEK-2 and psiCHEK-2-TAAL and grown under hyperglycemic (25 mM D-glucose) and
671 normal conditions. Luciferase assays were performed after 48 hrs of transfection according to the
672 manufacturer's protocol (Promega).

673 **Calcium imaging**

674 Calcium imaging was performed as previously described (Arora *et al*, 2021; Motiani *et al*, 2018).
675 Briefly, HUVEC-hTert2 cells, after knockdown and overexpression of lncRNA *TAAL*, were plated
676 on confocal dishes (SPL Life Sciences, Korea). After 48 hours of transfection, the cells were
677 incubated with 4 μM fura-2 AM for 30 minutes at 37°C. The cells were then washed three times
678 with HEPES-buffered saline solution (140 mM NaCl, 1.13 mM MgCl2, 4.7 mM KCl, 2 mM CaCl2,
679 10 mM D-glucose, and 10 mM HEPES; pH 7.4) and bathed for 5 minutes. For calcium imaging,
680 a Nikon Eclipse Ti2 microscope coupled with a CoolLED pE-340 Fura light source and a
681 high-speed PCO camera was used. Excitation was alternated at 340 and 380 nm, and emission
682 was captured at 510 nm. The cells were treated with 10 μM thapsigargin to observe calcium
683 release from the endoplasmic reticulum.

684 **Expression analysis in human blood samples**

685 Blood samples were collected in EDTA-coated vials (for RNA isolation) from individuals with
686 idiopathic macular holes and cataracts as normal controls for this study (n=60). Individuals with
687 diabetic duration of more than 5 and no diabetic retinopathy served as diabetic controls for the
688 study (n=50). Individuals with different forms of DR; mild NPDR (n=20), moderate NPDR
689 (n=25), severe NPDR (n=25) and PDR (n=50) were recruited as cases for this study. Sample
690 demographics are provided in the supply table 2. RNA was isolated from serum. The clot
691 activator vials containing 1 ml blood samples were centrifuged at 1200 rpm for 10 minutes at 4
692 degrees Celsius and the supernatant was collected and stored at -80 degree Celsius until further
693 use. The EDTA coated vials (containing 2 ml blood for RNA isolation) were subjected to series
694 of incubations using the erythrocyte lysis buffer to get rid of red blood cell content and obtain a
695 clear white pellet of white blood cells. RNA was extracted by the organic method using TRIzoL
696 reagent from WBC pellet from blood. Quality and quantity were assessed by agarose gel and

697 nanodrop spectrophotometer respectively. 500 ng of RNA was further reverse-transcribed to
698 cDNA using the Verso cDNA Synthesis Kit (AB1453B). Semi-quantitative PCR was carried out
699 using DyNAmo ColorFlash SYBR Green qPCR Kit (F-416L) and specific primers for lncRNA
700 TAAL. β-actin was used as an endogenous control. Statistical analysis was performed using the
701 student's t-test.
702

703 **Data Availability**

704 All the data has been provided in a supplementary file. Raw sequencing files will be shared upon
705 request.

706 **Conflict of Interest Disclosure**

707 The author declares no conflict of interest

708 **Acknowledgments**

709 This work was funded by DBT/Wellcome Trust India Alliance Fellowship (IA/I/19/2/504651)
710 awarded to Rajender K Motiani. SA acknowledges Senior Research Fellowships from DBT. The
711 authors want to acknowledge Dr. Soumya Sinha Roy and Dr. Barun Chatterjee for their valuable
712 input in cell culture work. We also like to acknowledge Dr. Jyoti Tanwar for assistance and input
713 with calcium imaging and Kriti Khare for assistance with confocal imaging. We also
714 acknowledge the CSIR-IGIB common instrumentation facility, and the ATPC confocal facility,
715 the FACS facility and all the LCSP lab members. Illustrations were made using BioRender.
716

717 **Author's contribution**

718 GR, SSB, RKM conceived and designed the experiment. GR, SA, LS, RB performed the
719 experiments and bioinformatic analysis. SS, SC, IK performed clinical experiments. GR, SSB,

and RKM analyzed the results. GR wrote the initial draft manuscript, and GR, SA, SSB, RKM edited the manuscript.

Reference

Abu Ahmad Y, Oknin-Vaisman A, Bitman-Lotan E & Orian A (2021) From the Evasion of Degradation to Ubiquitin-Dependent Protein Stabilization. *Cells* 10

Anders S, Pyl PT & Huber W (2015) HTSeq--a Python framework to work with high-throughput sequencing data. *Bioinformatics* 31: 166–169

Arora S, Tanwar J, Sharma N, Saurav S & Motiani RK (2021) Orai3 Regulates Pancreatic Cancer Metastasis by Encoding a Functional Store Operated Calcium Entry Channel. *Cancers* 13

Augustin HG, Koh GY, Thurston G & Alitalo K (2009) Control of vascular morphogenesis and homeostasis through the angiopoietin-Tie system. *Nat Rev Mol Cell Biol* 10: 165–177

Bates DO & Curry FE (1997) Vascular endothelial growth factor increases microvascular permeability via a Ca(2+)-dependent pathway. *American Journal of Physiology-Heart and Circulatory Physiology*

Cao X, Li T, Xu B, Ding K, Li W, Shen B, Chu M, Zhu D, Rui L, Shang Z, *et al* (2023) Endothelial TIE1 Restricts Angiogenic Sprouting to Coordinate Vein Assembly in Synergy With Its Homologue TIE2. *Arterioscler Thromb Vasc Biol* 43: e323–e338

Carlantoni C, Allanki S, Kontarakis Z, Rossi A, Piesker J, Günther S & Stainier DYR (2021) Tie1 regulates zebrafish cardiac morphogenesis through Tolloid-like 1 expression. *Dev Biol* 469: 54–67

Chatterjee B, Fatima F, Seth S & Sinha Roy S (2024) Moderate Elevation of Homocysteine Induces Endothelial Dysfunction through Adaptive UPR Activation and Metabolic Rewiring. *Cells* 13

Cheng H-T & Hung W-C (2013) Inhibition of proliferation, sprouting, tube formation and Tie2 signaling of lymphatic endothelial cells by the histone deacetylase inhibitor SAHA. *Oncol Rep* 30: 961–967

Chen Y, Li X, Li B, Wang H, Li M, Huang S, Sun Y, Chen G, Si X, Huang C, *et al* (2019) Long Non-coding RNA ECRAR Triggers Post-natal Myocardial Regeneration by Activating ERK1/2 Signaling. *Mol Ther* 27: 29–45

Dalal PJ, Muller WA & Sullivan DP (2020) Endothelial Cell Calcium Signaling during Barrier Function and Inflammation. *Am J Pathol* 190: 535–542

D'Amico G, Korhonen EA, Waltari M, Saharinen P, Laakkonen P & Alitalo K (2010) Loss of Endothelial Tie1 Receptor Impairs Lymphatic Vessel Development-Brief Report. *Arterioscler Thromb Vasc Biol*

Diederichs S (2014) The four dimensions of noncoding RNA conservation. *Trends Genet* 30:

757 121–123

758 Dobin A, Davis CA, Schlesinger F, Drenkow J, Zaleski C, Jha S, Batut P, Chaisson M &
759 Gingeras TR (2013) STAR: ultrafast universal RNA-seq aligner. *Bioinformatics* 29: 15–21

760 Duh EJ, Sun JK & Stitt AW (2017) Diabetic retinopathy: current understanding, mechanisms,
761 and treatment strategies. *JCI Insight* 2

762 ENCODE Project Consortium, Moore JE, Purcaro MJ, Pratt HE, Epstein CB, Shoresh N, Adrian
763 J, Kawli T, Davis CA, Dobin A, *et al* (2020) Expanded encyclopaedias of DNA elements in
764 the human and mouse genomes. *Nature* 583: 699–710

765 Fang S, Zhang L, Guo J, Niu Y, Wu Y, Li H, Zhao L, Li X, Teng X, Sun X, *et al* (2018)
766 NONCODEV5: a comprehensive annotation database for long non-coding RNAs. *Nucleic*
767 *Acids Res* 46: D308–D314

768 Ferraro NM, Strober BJ, Einson J, Abell NS, Aguet F, Barbeira AN, Brandt M, Bucan M, Castel
769 SE, Davis JR, *et al* (2020) Transcriptomic signatures across human tissues identify
770 functional rare genetic variation. *Science* 369

771 Gavard J (2013) Endothelial permeability and VE-cadherin: a wacky comradeship. *Cell Adh*
772 *Migr* 7: 455–461

773 Gu Y, Becker V, Qiu M, Tang T, Ampofo E, Menger MD & Laschke MW (2022) Brassinin
774 Promotes the Degradation of Tie2 and FGFR1 in Endothelial Cells and Inhibits
775 Triple-Negative Breast Cancer Angiogenesis. *Cancers* 14

776 Habeck H, Odenthal J, Walderich B, Maischein H, Schulte-Merker S & Tübingen 2000 screen
777 consortium (2002) Analysis of a zebrafish VEGF receptor mutant reveals specific
778 disruption of angiogenesis. *Curr Biol* 12: 1405–1412

779 Hamdollah Zadeh MA, Glass CA, Magnussen A, Hancox JC & Bates DO (2008)
780 VEGF-mediated elevated intracellular calcium and angiogenesis in human microvascular
781 endothelial cells in vitro are inhibited by dominant negative TRPC6. *Microcirculation* 15:
782 605–614

783 Hong S-Y, Kao Y-R, Lee T-C & Wu C-W (2018) Upregulation of E3 Ubiquitin Ligase CBLC
784 Enhances EGFR Dysregulation and Signaling in Lung Adenocarcinoma. *Cancer Res* 78:
785 4984–4996

786 Huang H, Bhat A, Woodnutt G & Lappe R (2010) Targeting the ANGPT-TIE2 pathway in
787 malignancy. *Nat Rev Cancer* 10: 575–585

788 Joussen AM, Ricci F, Paris LP, Korn C, Quezada-Ruiz C & Zarbin M (2021) Angiopoietin/Tie2
789 signalling and its role in retinal and choroidal vascular diseases: a review of preclinical data.
790 *Eye* 35: 1305–1316

791 Kang Y-J, Yang D-C, Kong L, Hou M, Meng Y-Q, Wei L & Gao G (2017) CPC2: a fast and

792 accurate coding potential calculator based on sequence intrinsic features. *Nucleic Acids Res*
793 45: W12–W16

794 Karner H, Webb C-H, Carmona S, Liu Y, Lin B, Erhard M, Chan D, Baldi P, Spitale RC & Sun S
795 (2020) Functional Conservation of LncRNA JPX Despite Sequence and Structural
796 Divergence. *J Mol Biol* 432: 283–300

797 Kreitman M, Noronha A & Yarden Y (2018) Irreversible modifications of receptor tyrosine
798 kinases. *FEBS Lett* 592: 2199–2212

799 Lalwani MK, Sharma M, Singh AR, Chauhan RK, Patowary A, Singh N, Scaria V & Sivasubbu
800 S (2012) Reverse genetics screen in zebrafish identifies a role of miR-142a-3p in vascular
801 development and integrity. *PLoS One* 7: e52588

802 La Porta S, Roth L, Singhal M, Mogler C, Spegg C, Schieb B, Qu X, Adams RH, Baldwin HS,
803 Savant S, *et al* (2018) Endothelial Tie1-mediated angiogenesis and vascular
804 abnormalization promote tumor progression and metastasis. *J Clin Invest* 128: 834–845

805 Lawson ND & Weinstein BM (2002) In vivo imaging of embryonic vascular development using
806 transgenic zebrafish. *Dev Biol* 248: 307–318

807 Lin A, Li C, Xing Z, Hu Q, Liang K, Han L, Wang C, Hawke DH, Wang S, Zhang Y, *et al* (2016)
808 The LINK-A lncRNA activates normoxic HIF1α signalling in triple-negative breast cancer.
809 *Nat Cell Biol* 18: 213–224

810 Liu J, Liu Z-X, Wu Q-N, Lu Y-X, Wong C-W, Miao L, Wang Y, Wang Z, Jin Y, He M-M, *et al*
811 (2020) Long noncoding RNA AGPG regulates PFKFB3-mediated tumor glycolytic
812 reprogramming. *Nat Commun* 11: 1507

813 Li X, Jiang W & Fang M (2023) An optimized protocol to detect ubiquitination modification of
814 exogenous or endogenous proteins. *STAR Protoc* 4: 102650

815 Motiani RK, Tanwar J, Raja DA, Vashisht A, Khanna S, Sharma S, Srivastava S, Sivasubbu S,
816 Natarajan VT & Gokhale RS (2018) STIM1 activation of adenylyl cyclase 6 connects Ca
817 and cAMP signaling during melanogenesis. *EMBO J* 37

818 Mueller SB & Kontos CD (2016) Tie1: an orphan receptor provides context for
819 angiopoietin-2/Tie2 signaling. *J Clin Invest* 126: 3188–3191

820 Pafumi I, Favia A, Gambara G, Papacci F, Ziparo E, Palombi F & Filippini A (2015) Regulation
821 of Angiogenic Functions by Angiopoietins through Calcium-Dependent Signaling
822 Pathways. *Biomed Res Int* 2015: 965271

823 Papapetropoulos A, Fulton D, Mahboubi K, Kalb RG, O'Connor DS, Li F, Altieri DC & Sessa
824 WC (2000) Angiopoietin-1 inhibits endothelial cell apoptosis via the Akt/survivin pathway.
825 *J Biol Chem* 275: 9102–9105

826 Pauli A, Valen E, Lin MF, Garber M, Vastenhouw NL, Levin JZ, Fan L, Sandelin A, Rinn JL,

827 Regev A, *et al* (2012) Systematic identification of long noncoding RNAs expressed during
828 zebrafish embryogenesis. *Genome Res* 22: 577–591

829 Phoenix KN, Yue Z, Yue L, Cronin CG, Liang BT, Hoeppner LH & Claffey KP (2022) PLCβ2
830 Promotes VEGF-Induced Vascular Permeability. *Arterioscler Thromb Vasc Biol* 42:
831 1229–1241

832 Ranjan G, Scaria V & Sivasubbu S (2024) Syntenic lncRNAs exhibit DNA regulatory functions
833 with sequence evolution. *bioRxiv*

834 Ranjan G, Sehgal P, Sharma D, Scaria V & Sivasubbu S (2021) Functional long non-coding and
835 circular RNAs in zebrafish. *Brief Funct Genomics*

836 Reinardy JL, Corey DM, Golzio C, Mueller SB, Katsanis N & Kontos CD (2015)
837 Phosphorylation of Threonine 794 on Tie1 by Rac1/PAK1 Reveals a Novel Angiogenesis
838 Regulatory Pathway. *PLoS One* 10: e0139614

839 Saharinen P, Eklund L & Alitalo K (2017) Therapeutic targeting of the angiopoietin-TIE
840 pathway. *Nat Rev Drug Discov* 16: 635–661

841 Saharinen P, Eklund L, Miettinen J, Wirkkala R, Anisimov A, Winderlich M, Nottebaum A,
842 Vestweber D, Deutsch U, Koh GY, *et al* (2008) Angiopoietins assemble distinct Tie2
843 signalling complexes in endothelial cell-cell and cell-matrix contacts. *Nat Cell Biol* 10:
844 527–537

845 Sahu SU, Visetsouk MR, Garde RJ, Hennes L, Kwas C & Gutzman JH (2017) Calcium signals
846 drive cell shape changes during zebrafish midbrain-hindbrain boundary formation. *Mol Biol*
847 *Cell* 28: 875–882

848 Sandoval R, Malik AB, Minshall RD, Kouklis P, Ellis CA & Tiruppathi C (2001) Ca(2+)
849 signalling and PKCalpha activate increased endothelial permeability by disassembly of
850 VE-cadherin junctions. *J Physiol* 533: 433–445

851 Sang L-J, Ju H-Q, Liu G-P, Tian T, Ma G-L, Lu Y-X, Liu Z-X, Pan R-L, Li R-H, Piao H-L, *et al*
852 (2018) LncRNA CamK-A Regulates Ca-Signaling-Mediated Tumor Microenvironment
853 Remodeling. *Mol Cell* 72: 601

854 Sato TN, Tozawa Y, Deutsch U, Wolburg-Buchholz K, Fujiwara Y, Gendron-Maguire M, Gridley
855 T, Wolburg H, Risau W & Qin Y (1995) Distinct roles of the receptor tyrosine kinases Tie-1
856 and Tie-2 in blood vessel formation. *Nature* 376: 70–74

857 Savant S, La Porta S, Budnik A, Busch K, Hu J, Tisch N, Korn C, Valls AF, Benest AV, Terhardt
858 D, *et al* (2015) The Orphan Receptor Tie1 Controls Angiogenesis and Vascular Remodeling
859 by Differentially Regulating Tie2 in Tip and Stalk Cells. *Cell Rep* 12: 1761–1773

860 Saw PE & Song E (2024) Advancements in clinical RNA therapeutics: Present developments
861 and prospective outlooks. *Cell Rep Med* 5: 101555

Schindelin J, Arganda-Carreras I, Frise E, Kaynig V, Longair M, Pietzsch T, Preibisch S, Rueden C, Saalfeld S, Schmid B, *et al* (2012) Fiji: an open-source platform for biological-image analysis. *Nat Methods* 9: 676–682

Sehgal P, Mathew S, Sivadas A, Ray A, Tanwar J, Vishwakarma S, Ranjan G, Shamsudheen KV, Bhoyar RC, Pateria A, *et al* (2021) LncRNA VEAL2 regulates PRKCB2 to modulate endothelial permeability in diabetic retinopathy. *EMBO J* 40: e107134

Shinde AV, Motiani RK, Zhang X, Abdullaev IF, Adam AP, González-Cobos JC, Zhang W, Matrougui K, Vincent PA & Trebak M (2013) STIM1 controls endothelial barrier function independently of Orai1 and Ca2+ entry. *Sci Signal* 6: ra18

Singhal M, Gengenbacher N, La Porta S, Gehrs S, Shi J, Kamiyama M, Bodenmiller DM, Fischl A, Schieb B, Besemfelder E, *et al* (2020) Preclinical validation of a novel metastasis-inhibiting Tie1 function-blocking antibody. *EMBO Mol Med* 12: e11164

Sparmann A & Vogel J (2023) RNA-based medicine: from molecular mechanisms to therapy. *EMBO J* 42: e114760

Stolz B & Bereiter-Hahn J (1988) Increase of cytosolic calcium results in formation of F-actin aggregates in endothelial cells. *Cell Biol Int Rep* 12: 321–329

Takano H, Murasawa S & Asahara T (2008) Functional and gene expression analysis of hTERT overexpressed endothelial cells. *Biologics* 2: 547–554

Ten S, Hodge K & I. A (2012) Dynamic proteomics: Methodologies and analysis. In *Functional Genomics* InTech

Tiruppathi C, Minshall RD, Paria BC, Vogel SM & Malik AB (2002) Role of Ca2+ signaling in the regulation of endothelial permeability. *Vascul Pharmacol* 39: 173–185

Tracz M & Bialek W (2021) Beyond K48 and K63: non-canonical protein ubiquitination. *Cell Mol Biol Lett* 26: 1

Traver D, Paw BH, Poss KD, Penberthy WT, Lin S & Zon LI (2003) Transplantation and in vivo imaging of multilineage engraftment in zebrafish bloodless mutants. *Nat Immunol* 4: 1238–1246

Tsai F-C & Meyer T (2012) Ca2+ pulses control local cycles of lamellipodia retraction and adhesion along the front of migrating cells. *Curr Biol* 22: 837–842

Tsai F-C, Seki A, Yang HW, Hayer A, Carrasco S, Malmersjö S & Meyer T (2014) A polarized Ca2+, diacylglycerol and STIM1 signalling system regulates directed cell migration. *Nat Cell Biol* 16: 133–144

Ulitsky I (2016) Evolution to the rescue: using comparative genomics to understand long non-coding RNAs. *Nat Rev Genet* 17: 601–614

Wang L, Park HJ, Dasari S, Wang S, Kocher J-P & Li W (2013) CPAT: Coding-Potential Assessment Tool using an alignment-free logistic regression model. *Nucleic Acids Res* 41: e74

Wehrle C, Van Slyke P & Dumont DJ (2009) Angiopoietin-1-induced ubiquitylation of Tie2 by c-Cbl is required for internalization and degradation. *Biochem J* 423: 375–380

Wong TY, Cheung CMG, Larsen M, Sharma S & Simó R (2016) Diabetic retinopathy. *Nature Reviews Disease Primers* 2: 1–17

Xu M, Xu H-H, Lin Y, Sun X, Wang L-J, Fang Z-P, Su X-H, Liang X-J, Hu Y, Liu Z-M, *et al* (2019) LECT2, a Ligand for Tie1, Plays a Crucial Role in Liver Fibrogenesis. *Cell* 178: 1478–1492.e20

Yang H, Luan Y, Liu T, Lee HJ, Fang L, Wang Y, Wang X, Zhang B, Jin Q, Ang KC, *et al* (2020) A map of cis-regulatory elements and 3D genome structures in zebrafish. *Nature* 588: 337–343

Yu T, Zhao Y, Hu Z, Li J, Chu D, Zhang J, Li Z, Chen B, Zhang X, Pan H, *et al* (2017) MetaLnc9 Facilitates Lung Cancer Metastasis via a PGK1-Activated AKT/mTOR Pathway. *Cancer Res* 77: 5782–5794

Zhao L, Zhao J, Zhong K, Tong A & Jia D (2022) Targeted protein degradation: mechanisms, strategies and application. *Signal Transduct Target Ther* 7: 113

Zhou L, Liu R, Liang X, Zhang S, Bi W, Yang M, He Y, Jin J, Li S, Yang X, *et al* (2020) lncRNA RP11-624L4.1 Is Associated with Unfavorable Prognosis and Promotes Proliferation via the CDK4/6-Cyclin D1-Rb-E2F1 Pathway in NPC. *Mol Ther Nucleic Acids* 22: 1025–1039

Zhu Y, Zhu L, Wang X & Jin H (2022) RNA-based therapeutics: an overview and prospectus. *Cell Death Dis* 13: 644

Figure legends

Figure 1: *Tie1-associated angiogenic lncRNA (TAAL)* interaction *Tie1* protein.

[A] Schematic of RNA-immunoprecipitation pipeline for Tie1 protein using HUVEC-hTert2 cell line.

[B] Differential expression analysis of *Tie1/IgG* revealed one enriched lncRNA with a fold change greater than 5, represented in red.

[C] UCSC genome browser snapshot of *TAAL lncRNA* locus in human.

[D] The bar plot represents RNA-immunoprecipitation of *Tie2* in HUVEC-hTert2 cells and shows no enrichment of lncRNA *TAAL.* Data from 3 independent biological replicates plotted as

929 mean fold change ± standard deviation . ns- not significant (two-tailed unpaired t-test)
930 [E] The bar plot depicts the relative abundance of Tie1, Tie2, *TAAL*, GAPDH, β-actin, and
931 MALAT1 in various subcellular fractions quantified using qRT-PCR. *TAAL*, GAPDH, and
932 β-actin show enrichment in the cytoplasmic fraction. Tie1 and Tie2 exhibit equal enrichment in
933 both the cytoplasm and nucleus, while *MALAT1* is predominantly enriched in the nucleus. The
934 data represent relative abundance percentages ± SEM from three independent experiments.
935 [F] Single molecular FISH (smFISH) of *TAAL* (610nM) and Co-IF for Tie1 (GFP) and Tie2
936 (Magenta) highlight their colocalization. Magnification-60x
937
938 **Figure 2: lncRNA *TAAL* modulates pathophysiological function in endothelial cells.**
939 [A-B] Box and whisker plot representing quantification of wound closer rate in scratch wound
940 assay after 24 hrs in control and *TAAL* knockdown or overexpressed cells. *** p-value ≤ 0.001 ;
941 **** p-value ≤ 0.0001. (two-tailed unpaired t-test).
942 [C-D] Bar plot representing quantification of cells migration in the transwell assay compared in
943 control and *TAAL* knockdown or overexpressed cells.* p-value ≤ 0.05; ** p-value ≤ 0.01
944 (two-tailed unpaired t-test).
945 [E-F] Bar plot representing quantification of absorbance in the BrdU proliferation assay
946 compared in control and *TAAL* knockdown or overexpressed cells. ** p-value ≤ 0.01 (two-tailed
947 unpaired t-test).
948 [G-H]Knockdown and overexpression of *TAAL* significantly alter the permeability of
949 dextran-conjugated FITC. Bar plot representing relative dextran-FITC efflux in control and
950 *TAAL* knockdown or overexpressed cells. * p-value ≤ 0.05. (two-tailed unpaired t-test).
951 [I]Knockdown and overexpression of *TAAL* in HUVECs exhibited a reduction in tube formation
952 in Matrigel when compared to the control.
953 [J] Box and whisker plot representing quantification of the number of branched vessels in *TAAL*
954 knockdown (siTAAL) and overexpressed (pcDNA-TAAL) cells along with their controls (
955 siControl; pcDNA3.1). *** p-value ≤ 0.001, **** p-value ≤ 0.0001. (two-tailed unpaired t-test).
956 [K-L] Flow cytometry analysis of cell viability, stained by Annexin V (Q3) and PI (Q1) with
957 viable cells which are negative for both Annexin V and PI (Q4) in control and *TAAL* lncRNA
958 knockdown or overexpression cells.
959

Figure 3: LncRNA *TAAL* modulates cytoskeleton dynamics by altering calcium levels.

[A] Knockdown and overexpression of *TAAL* significantly alter the cytoskeleton dynamics in HUVEC cells. Confocal images of F-actin stained with Alexa Fluor 488 phalloidin in control and *TAAL* knockdown or overexpressed cells (60X magnification). Dot plot representing quantification of aspect ratio (long/short axis) in control and *TAAL* knockdown or overexpressed cells.* p-value ≤ 0.05; ** p-value ≤ 0.01 (two-tailed unpaired t-test).

[B] Representation of Ca^{2+} imaging trace of control and *TAAL* knockdown HUVEC cells with stimulation with thapsigargin (Tg).

[C] Quantification of basal Ca^{2+} levels in control and *TAAL* knockdown HUVEC cells. * p-value ≤ 0.05. (two-tailed unpaired t-test).

[D]Quantification of Ca^{2+} levels release from the endoplasmic reticulum (ER) upon stimulation in Tg in control and *TAAL* knockdown HUVEC cells. *** p-value ≤ 0.001. (two-tailed unpaired t-test).

[E] Representation of Ca^{2+} imaging trace of control and *TAAL* overexpressed HUVEC cells with stimulation with Tg.

[F] Quantification of basal Ca^{2+} levels in control and *TAAL* overexpressed HUVEC cells. ** p-value ≤ 0.01. (two-tailed unpaired t-test).

[G]Quantification of Ca^{2+} levels release from ER upon stimulation in Tg in control and *TAAL* overexpressed HUVEC cells. ** p-value ≤ 0.01. (two-tailed unpaired t-test).

[H] Knockdown and overexpression of *TAAL* significantly alters the localization of VE-Cadhaerin at the junction of HUVEC cells. Confocal images of immunofluorescence VE-Cadhaerin in control and *TAAL* knockdown or overexpressed cells (60X magnification).

Figure 4: Conserved function of lncRNA *TAAL* in zebrafish regulates angiogenesis.

[A] Schematic of RNA-immunoprecipitation pipeline for *tie1* protein using24 hpf zebrfish embryos.

[B] Differential expression analysis of tie1/IgG revealed one enriched lncRNA (ZFLNCG0999) with a fold change greater than 4.5 and $\log_{10}$ P value greater thant 15, represented in red.

[C] Expression pattern of *taal* lncRNA, *tie1* and *tie2* (measured in TPM) across eight distinct developmental stages in zebrafish, utilizing publicly accessible RNA-seq data.

[D] Expression pattern of *taal* lncRNA, *tie1* and *tie2* (measured in TPM) across 12 different

991 tissues using publically available RNA-seq data.

992 [E] Representative images of cranial and trunk vasculature of control and morpholino mediated
993 *taal* knockdown Tg (fli1:eGFP) zebrafish at 24 hpf and 48 hpf at 5x magnification. Bar graph
994 represent quantification of angiogenic defects in control and *taal* knockdown zebrafish. Arrow
995 marks represent the defective angiogenic vessel. **** p-value ≤ 0.0001. (two-tailed unpaired
996 t-test).

997 [F] LncRNA *taal* knockdown enhances angiogesis in zebafish. Representative images of
998 angiogenic sprouting in control and morpholino *taal* injected at at subintestinal vessels (SIVs) in
999 Tg (fli1:eGFP) zebrafish. Complementation of human lncRNA *TAAL* in morpholino-*taal* injected
1000 Tg(fli1:eGFP) zebrafish at subintestinal vessels (SIVs) halted angiogenic sprouting. Arrow
1001 marks represent the sprouting vessels. Bar graph represent quantification of number of
1002 angiogenic sprotingin in control, *taal* knockdown and *taal* knockdown complimented with
1003 human *TAAL* in zebrafish. ns- not significant; ** p-value ≤ 0.01; *** p-value ≤ 0.001. (two-tailed
1004 unpaired t-test).

1005 [G] Representative images of trunk vasculature of control and *TAAL* overexpression (OE) in Tg
1006 (fli1:eGFP) zebrafish at 48 hpf with 5x magnification. Bar graph represent quantification of
1007 angiogenic defects in control and *TAAL* overexpressed zebrafish. Arrow marks represent the
1008 defective angiogenic vessel. **** p-value ≤ 0.0001. (two-tailed unpaired t-test).

1009 [F] Representative images of angiogenic sprouting in control and Overexpressed *TAAL* injected
1010 at at subintestinal vessels (SIVs) in Tg (fli1:eGFP) zebrafish. Box and whisker plot repent the
1011 area of SIVs in control and Overexpressed *TAAL* injected zebrafish. ** p-value ≤ 0.01
1012 (two-tailed unpaired t-test).

1013

1014 **Figure 5: LncRNA *TAAL* modulates *Tie1* and *Tie2* protein levels.**

1015 [A] Immunoblotting of Tie1 and Tie2 in control and TAAL knockdown or overexpressed cells.
1016 Bar plot representing quantification of blots. * p-value ≤ 0.05; ** p-value ≤ 0.01 (two-tailed
1017 unpaired t-test).

1018 [B] Bar plot representing relative fold change in mRNA expression levels of *Tie1* and *Tie2*
1019 between control and *TAAL* knockdown or overexpressed cells. ns- not significant (two-tailed
1020 unpaired t-test).

1021 [C] Knockdown and overexpression of *TAAL* significantly alters the protein levels of Tie1 and

1022 Tie2 in HUVEC cells. Confocal images of immunofluorescence Tie1 and Tie2 in control and
1023 *TAAL* knockdown or overexpressed cells (60X maginication).
1024
1025 **Figure 6: LncRNA *TAAL* controls the protein turnover of *Tie1* by modulating it**
1026 **ubiquitination.**
1027 [A] Schematic of Protomics quntificatino pipeline for ceontrol and TAAL knockdown cells.
1028 [B] Dot plot representing Gene ontology molecular process for protein downregulated in *TAAL*
1029 knockdown cells upon comparing to the control.
1030 [C] Dot plot representing Gene ontology molecular process for protein up-regulated in *TAAL*
1031 knockdown cells upon comparing to the control.
1032 [D] Immunobloting of *Tie1* protein upon treatment of cells with translational inhibitor
1033 cycloheximide (Chx) for 0, 4, 8 hrs in control and *TAAL* knockdown or overexpressed cells.
1034 GAPDH was used as an input control.
1035 [E] Immunobloting of *Tie1* protein upon treatment of cells with degradation inhbitor MG132 and
1036 bafilomycin A1(Baf) for 8 hrs in control and *TAAL* knockdown or overexpressed cells. GAPDH
1037 was used as an input control.
1038 [F] Change in polyubiqutination of *Tie1* and *Tie2* protein in *TAAL* knockdown or overexpressed
1039 cells. Lysates of control and *TAAL* knockdown or overexpressed cells cotrnasfected with
1040 HA-Ubiquitin vector were immunoprecipitated with *Tie1* and *Tie2* antibody and immunoblotted
1041 with anti-HA antibody.
1042 [G] Hypothetical schematic illustrating the protective effect of lncRNA TAAL on Tie1 through
1043 polyubiquitination with heterotypic chains, which attract ubiquitin-like proteins and prevent
1044 lysosomal degradation.
1045 **Figure 7: LncRNA *TAAL* plays a crucial role in regulating permeability and junctional**
1046 **dynamics in diabetic retinopathy.**
1047 [A] Bar graph representing relative fold change levels of TAAL, Tie1, Tie2 upon treatment with
1048 hyperglysemia compared to control. ns- not significant; **** p-value ≤ 0.0001. (two-tailed
1049 unpaired t-test).
1050 [B] Expression profile of *TAAL* lncRNA in exosomes from different cell lines represented in as a
1051 bar graph.
1052 [C] Schematics of blood collection and quantification of lncRNA *TAAL* in diabetic and

1053 non-diabetics individuals. Bar graph represents relative fold change expression of lncRNA *TAAL*
1054 in blood samples of control, diabetic mellitus (DM), non-poliferative diabetic retinopathy
1055 (NPDR) and polyfrerative diabetic retinopathy (PDR) patients.
1056 [D-E] ROC curve analysis determines the sensitivity and specificity of lncRNA *TAAL* as
1057 diagnostic biomarker for NPDR or PDR patients with vascular dysfunction.
1058 [F] Complimentation of *TAAL* lncRNA in HUVEC hyperglysemic model reverts the increased
1059 permeability. Bar graph represents retalive dextran-FITC efflux in control untreated, control
1060 hyperglycemic and *TAAL* overexpressed in hyperglycemic cells. **** p-value ≤ 0.0001.
1061 (two-tailed unpaired t-test).
1062 [G] Complimentation of *TAAL* lncRNA in HUVEC hyperglysemic model reverts the localisation
1063 of VE-Cadhaerin at the junction of HUVEC cells. Confocal images of immunofluorescence
1064 VE-Cadhaerin in control and *TAAL* overexpressed cells under hyperglycemic condition (60X
1065 maginication).
1066 [H] Complimentation of *TAAL* lncRNA in HUVEC hyperglysemic model reverts the *in-vivo*
1067 expression of *TAAL* by increasing its promoter activity. Luciferase assay of lncRNA *TAAL*
1068 promoter in control untreated, control hypoglycemics and *TAAL* overexpressed hyperglycemic
1069 cells represented in a bar graph. * p-value ≤ 0.05; ** p-value ≤ 0.01; *** p-value ≤ 0.001
1070 (two-tailed unpaired t-test).
1071 [I] Illustration showing lncRNA TAAL's role in controlling vascular permeability and junctional
1072 dynamics through the regulation of Tie1 levels in normal cells. In hyperglycemic conditions,
1073 cells downregulate lncRNA TAAL expression and exocytose the residual TAAL transcripts into
1074 the bloodstream.
1075
1076 **Figure 8: LncRNA *TAAL* controls the protein turnover of *Tie1* and modulates vascular**
1077 **permeability and angiogenic function.**
1078
1079
1080
1081

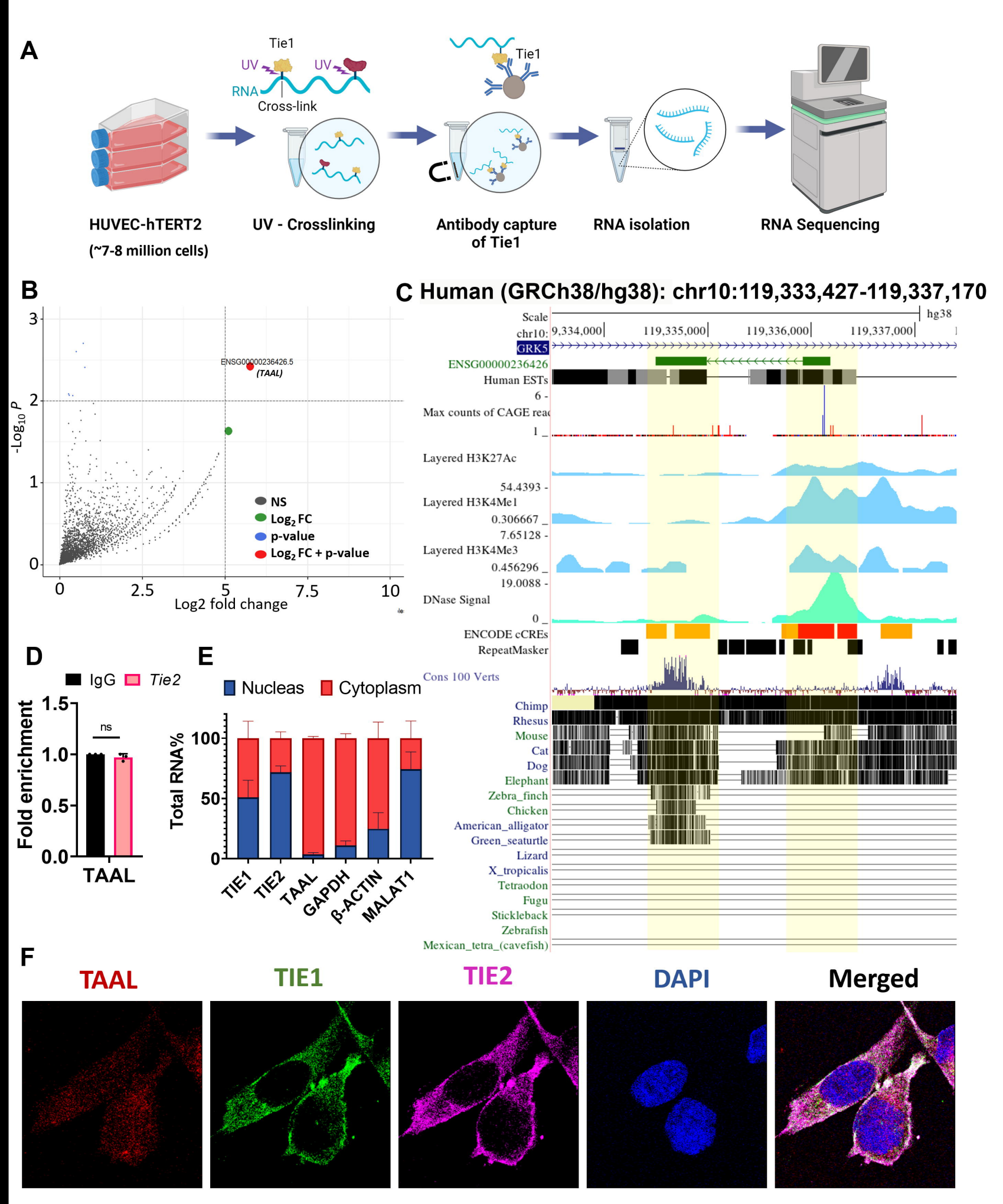
A
Tie1
UV
UV
RNA
Cross-link
Tie1
HUVEC-hTERT2
(~7-8 million cells)
UV - Crosslinking
Antibody capture of Tie1
RNA isolation
RNA Sequencing
B
ENSG00000236426.5
(TAAL)
-Log10 P
Log2 fold change
NS
Log2 FC
p-value
Log2 FC + p-value
C Human (GRCh38/hg38): chr10:119,333,427-119,337,170
Scale
chr10:
hg38
9,334,000
119,335,000
119,336,000
119,337,000
GRK5
ENSG00000236426
Human ESTs
Max counts of CAGE reads
Layered H3K27Ac
Layered H3K4Me1
Layered H3K4Me3
DNase Signal
ENCODE cCREs
RepeatMasker
Cons 100 Verts
Chimp
Rhesus
Mouse
Cat
Dog
Elephant
Zebra_finch
Chicken
American_alligator
Green_seaturtle
Lizard
X_tropicalis
Tetraodon
Fugu
Stickleback
Zebrafish
Mexican_tetra_(cavefish)
D
IgG
Tie2
Fold enrichment
ns
TAAL
E
Nucleas
Cytoplasm
Total RNA%
TIE1
TIE2
TAAL
GAPDH
β-ACTIN
MALAT1
F
TAAL
TIE1
TIE2
DAPI
Merged

Scratch wound assay

Transwell migration assay

A

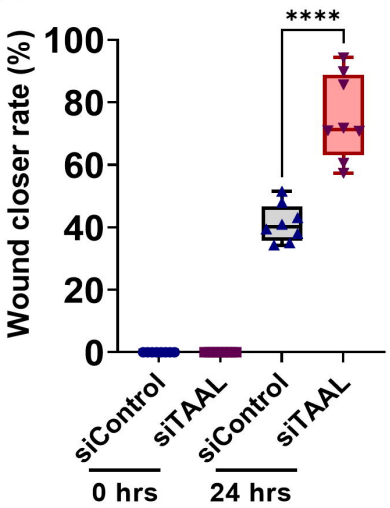

B

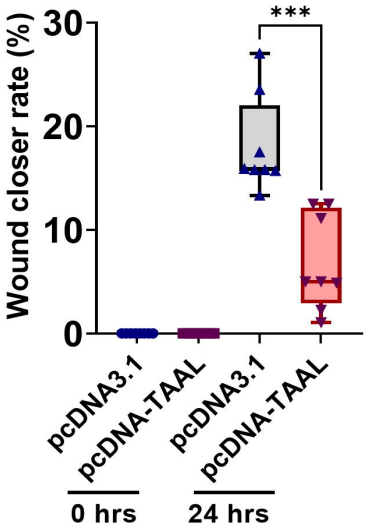

C

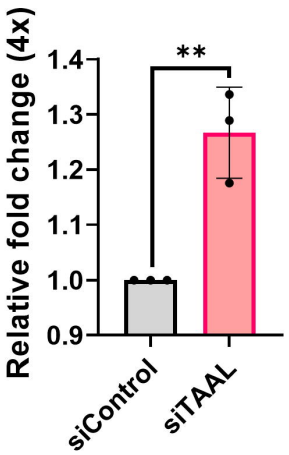

D

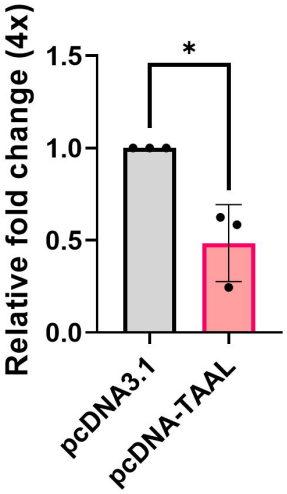

Permeability assay

E

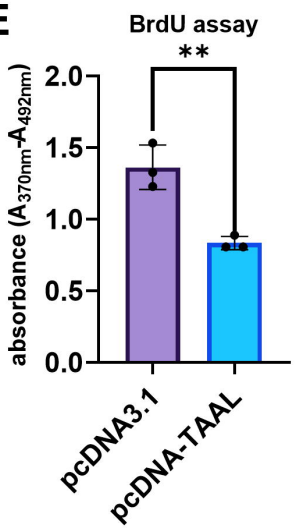

F

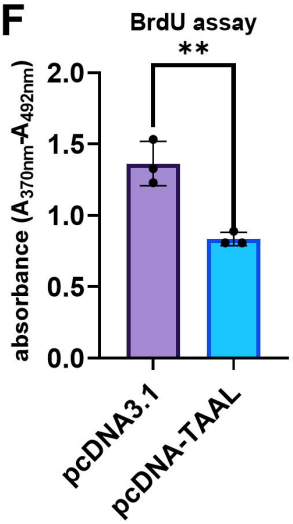

G

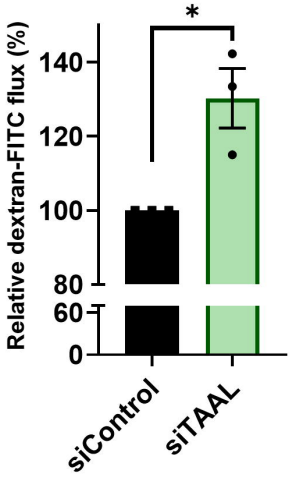

H

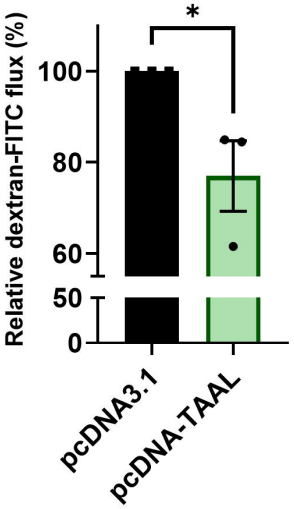

I

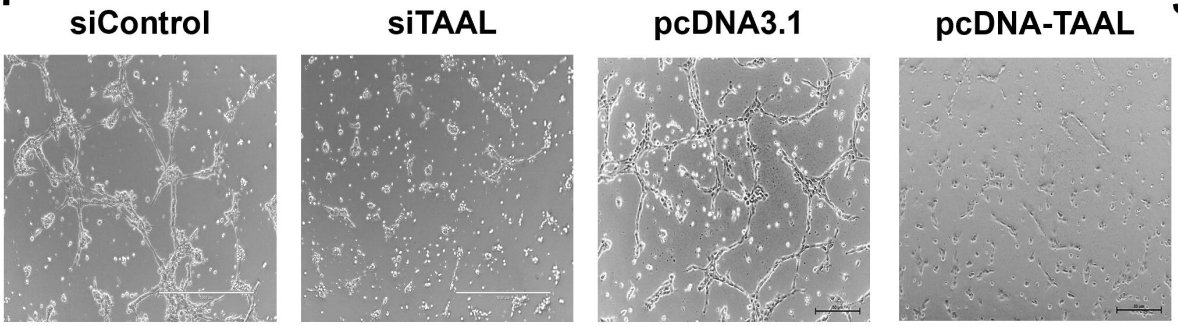

J

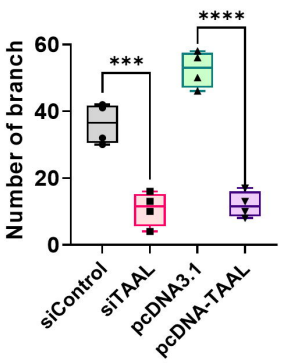

K

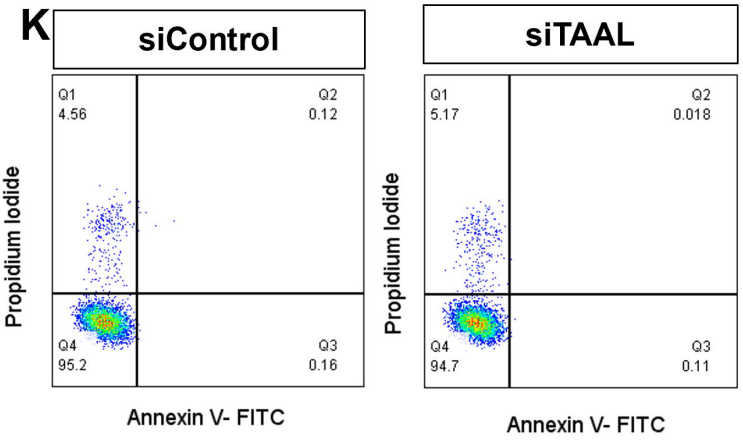

L

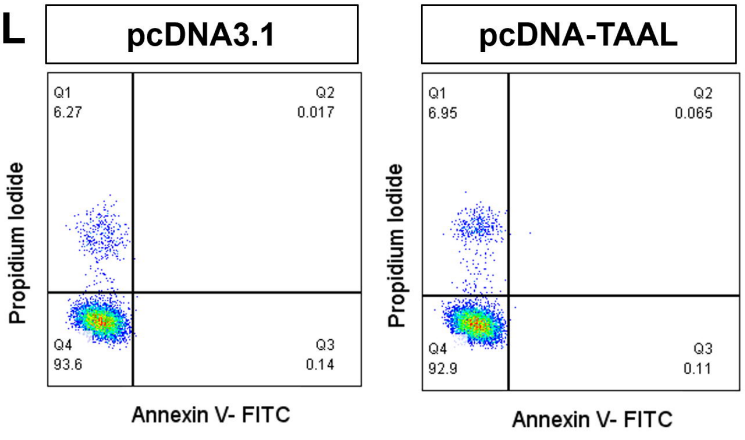

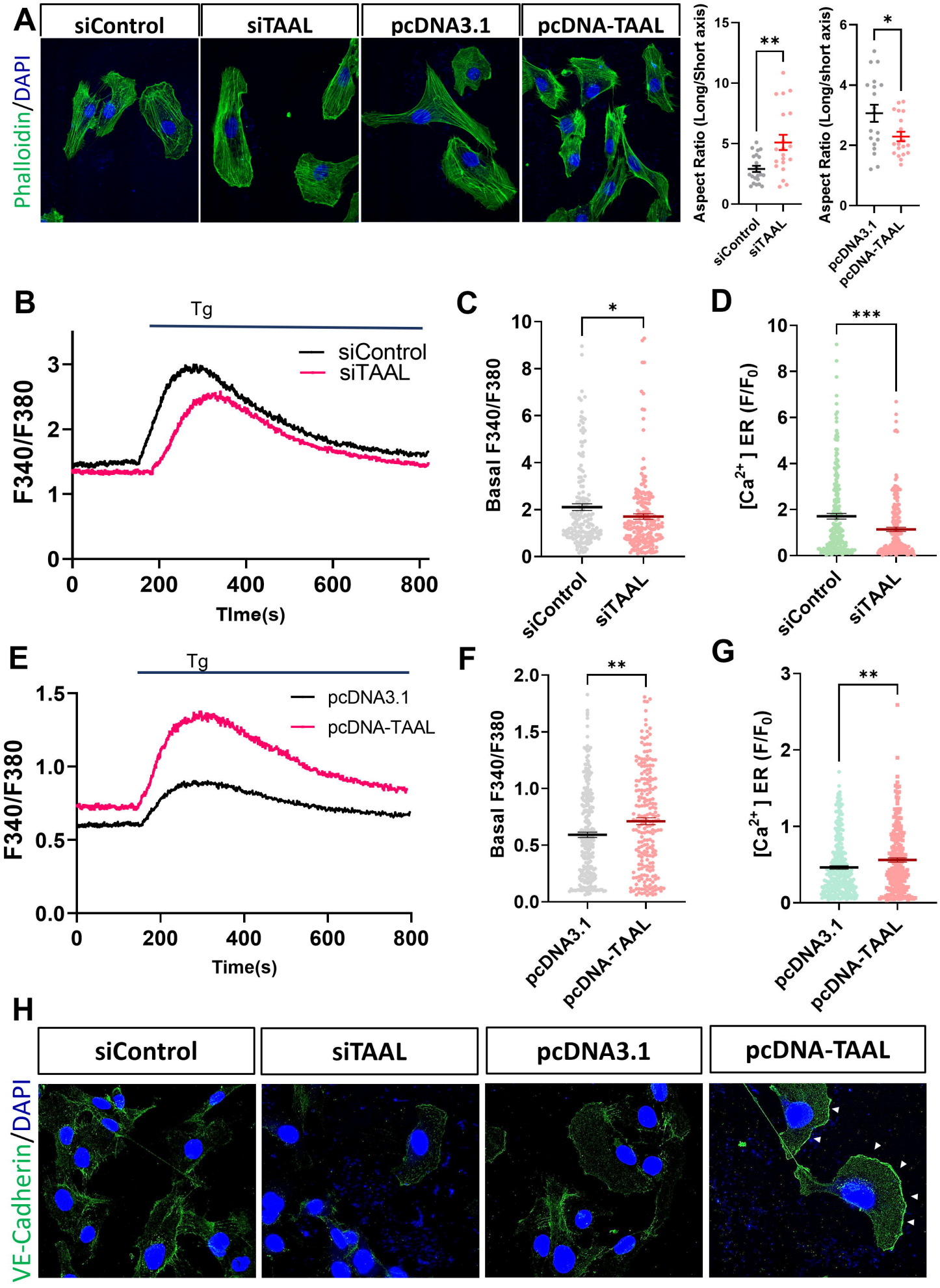
A
siControl
siTAAL
pcDNA3.1
pcDNA-TAAL
Phalloidin/DAPI
Aspect Ratio (Long/Short axis)
**
*
siControl
siTAAL
pcDNA3.1
pcDNA-TAAL
B
Tg
siControl
siTAAL
F340/F380
Time(s)
C
Basal F340/F380
*
D
[Ca2+] ER (F/F0)
***
E
Tg
pcDNA3.1
pcDNA-TAAL
F340/F380
Time(s)
F
Basal F340/F380
**
G
[Ca2+] ER (F/F0)
**
H
siControl
siTAAL
pcDNA3.1
pcDNA-TAAL
VE-Cadherin/DAPI

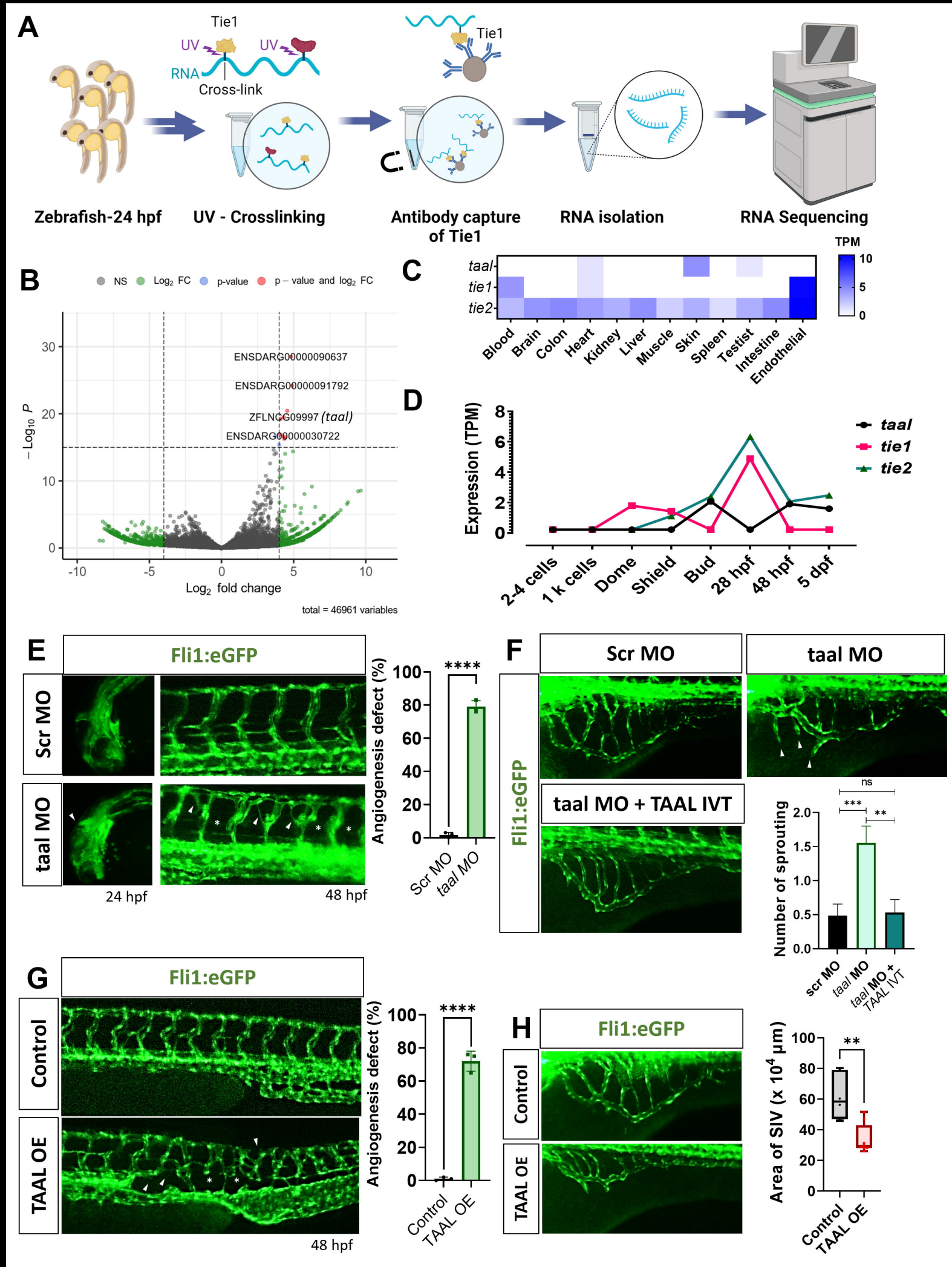
A
Tie1
UV
UV
RNA
Cross-link
Tie1
Zebrafish-24 hpf
UV - Crosslinking
Antibody capture of Tie1
RNA isolation
RNA Sequencing
B
NS
Log2 FC
p-value
p – value and log2 FC
ENSDARG00000090637
ENSDARG00000091792
ZFLNCG09997 (taal)
ENSDARG00000030722
– Log10 P
Log2 fold change
total = 46961 variables
C
TPM
taal
tie1
tie2
Blood
Brain
Colon
Heart
Kidney
Liver
Muscle
Skin
Spleen
Testist
Intestine
Endothelial
D
Expression (TPM)
taal
tie1
tie2
2-4 cells
1 k cells
Dome
Shield
Bud
28 hpf
48 hpf
5 dpf
E
Fli1:eGFP
Scr MO
taal MO
24 hpf
48 hpf
Angiogenesis defect (%)
****
Scr MO
taal MO
F
Scr MO
taal MO
Fli1:eGFP
taal MO + TAAL IVT
Number of sprouting
ns
***
**
scr MO
taal MO
taal MO + TAAL IVT
G
Fli1:eGFP
Control
TAAL OE
48 hpf
Angiogenesis defect (%)
****
Control
TAAL OE
H
Fli1:eGFP
Control
TAAL OE
Area of SIV (x 10^4 µm)
**
Control
TAAL OE

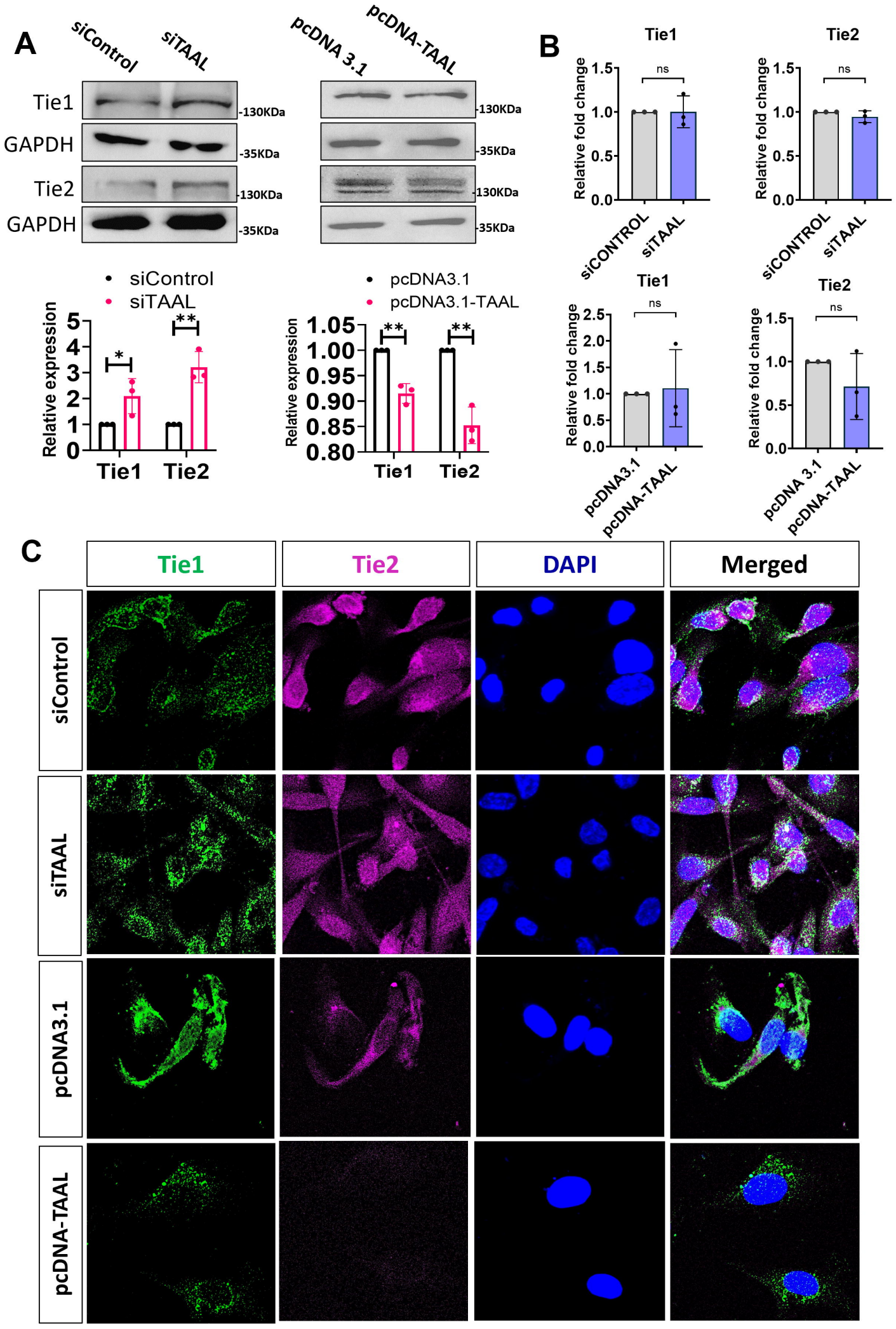
A
siControl
siTAAL
pcDNA 3.1
pcDNA-TAAL
Tie1
GAPDH
Tie2
GAPDH
130KDa
35KDa
siControl
siTAAL
Relative expression
Tie1
Tie2
pcDNA3.1
pcDNA3.1-TAAL
B
Tie1
Tie2
Relative fold change
ns
siCONTROL
siTAAL
pcDNA3.1
pcDNA-TAAL
C
Tie1
Tie2
DAPI
Merged
siControl
siTAAL
pcDNA3.1
pcDNA-TAAL

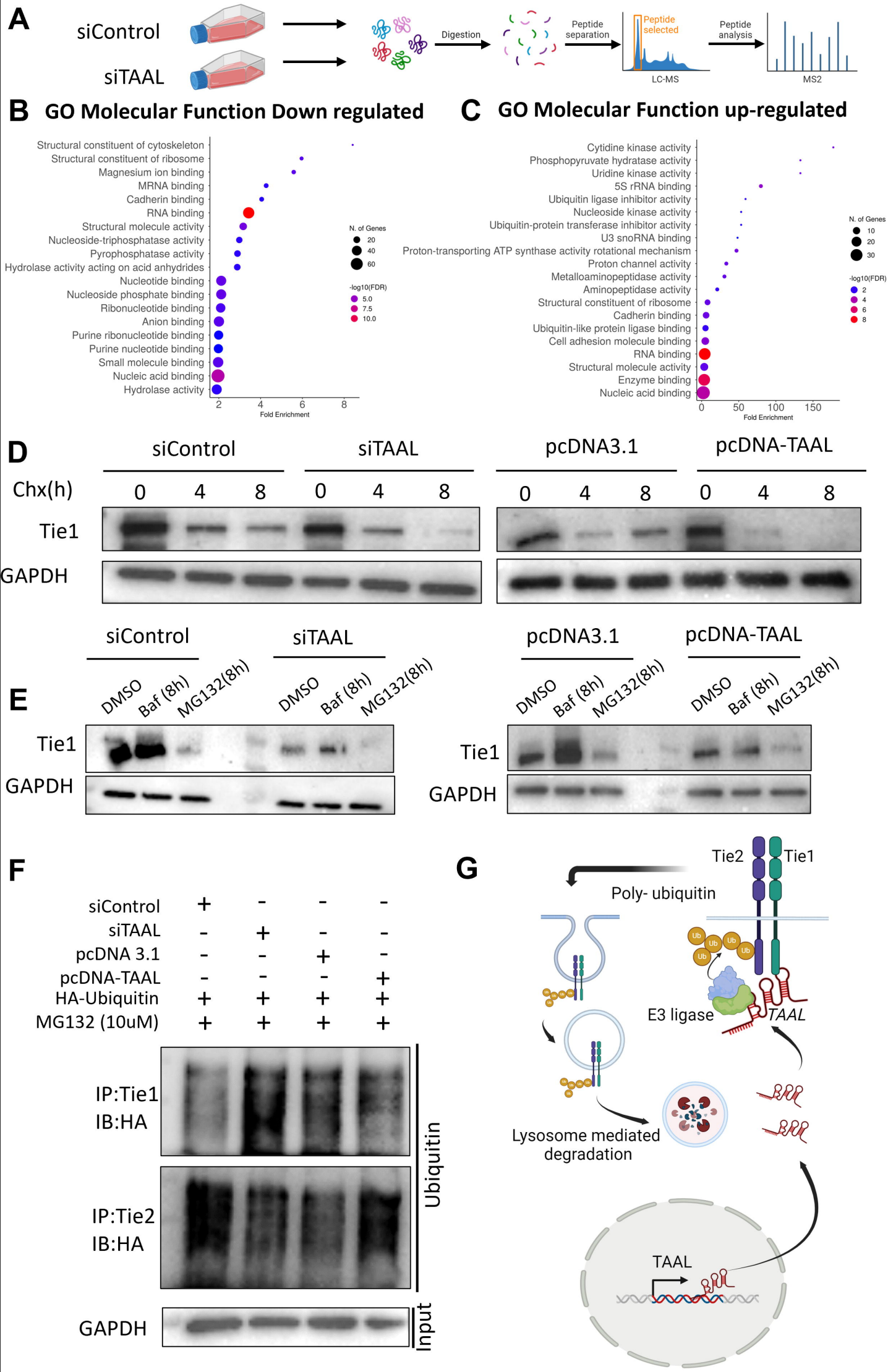
A
siControl
siTAAL
Digestion
Peptide separation
Peptide selected
LC-MS
Peptide analysis
MS2
B GO Molecular Function Down regulated
Structural constituent of cytoskeleton
Structural constituent of ribosome
Magnesium ion binding
MRNA binding
Cadherin binding
RNA binding
Structural molecule activity
Nucleoside-triphosphatase activity
Pyrophosphatase activity
Hydrolase activity acting on acid anhydrides
Nucleotide binding
Nucleoside phosphate binding
Ribonucleotide binding
Anion binding
Purine ribonucleotide binding
Purine nucleotide binding
Small molecule binding
Nucleic acid binding
Hydrolase activity
Fold Enrichment
N. of Genes
-log10(FDR)
C GO Molecular Function up-regulated
Cytidine kinase activity
Phosphopyruvate hydratase activity
Uridine kinase activity
5S rRNA binding
Ubiquitin ligase inhibitor activity
Nucleoside kinase activity
Ubiquitin-protein transferase inhibitor activity
U3 snoRNA binding
Proton-transporting ATP synthase activity rotational mechanism
Proton channel activity
Metalloaminopeptidase activity
Aminopeptidase activity
Structural constituent of ribosome
Cadherin binding
Ubiquitin-like protein ligase binding
Cell adhesion molecule binding
RNA binding
Structural molecule activity
Enzyme binding
Nucleic acid binding
Fold Enrichment
N. of Genes
-log10(FDR)
D
siControl
siTAAL
pcDNA3.1
pcDNA-TAAL
Chx(h)
0 4 8 0 4 8 0 4 8 0 4 8
Tie1
GAPDH
E
siControl
siTAAL
pcDNA3.1
pcDNA-TAAL
DMSO
Baf (8h)
MG132(8h)
Tie1
GAPDH
F
siControl + - - -
siTAAL - + - -
pcDNA 3.1 - - + -
pcDNA-TAAL - - - +
HA-Ubiquitin + + + +
MG132 (10uM) + + + +
IP:Tie1
IB:HA
IP:Tie2
IB:HA
Ubiquitin
GAPDH
Input
G
Tie2
Tie1
Poly- ubiquitin
Ub
E3 ligase
TAAL
Lysosome mediated degradation
TAAL

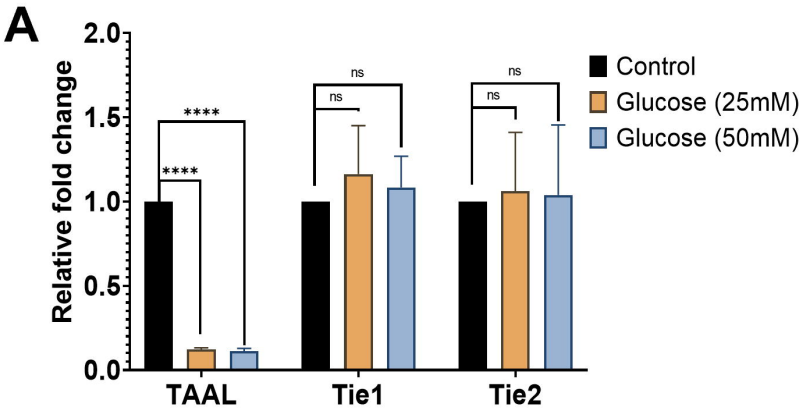
A
Relative fold change
2.0
1.5
1.0
0.5
0.0
****
****
ns
ns
ns
ns
Control
Glucose (25mM)
Glucose (50mM)
TAAL
Tie1
Tie2

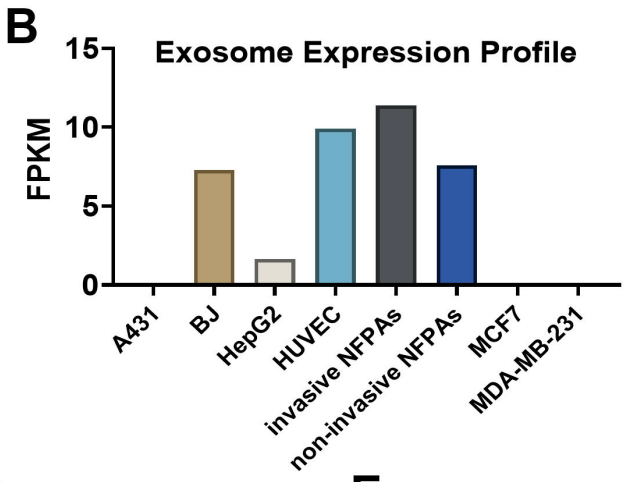
B
Exosome Expression Profile
FPKM
15
10
5
0
A431
BJ
HepG2
HUVEC
invasive NFPAs
non-invasive NFPAs
MCF7
MDA-MB-231

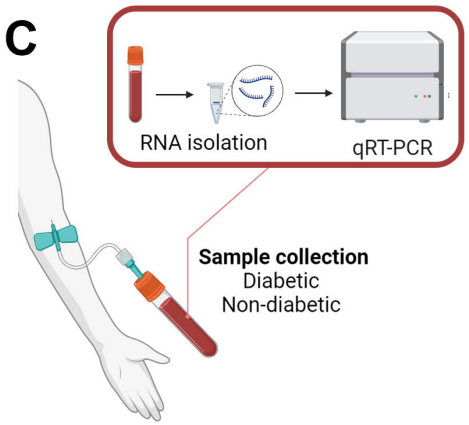
C
RNA isolation
qRT-PCR
Sample collection
Diabetic
Non-diabetic

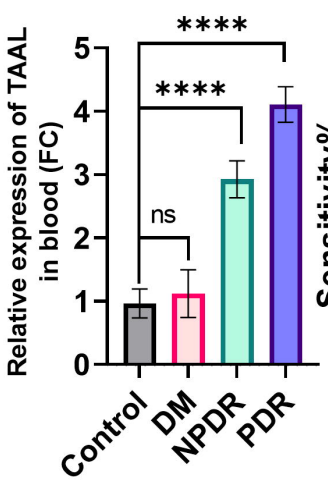
Relative expression of TAAL in blood (FC)
5
4
3
2
1
0
****
****
ns
Control
DM
NPDR
PDR

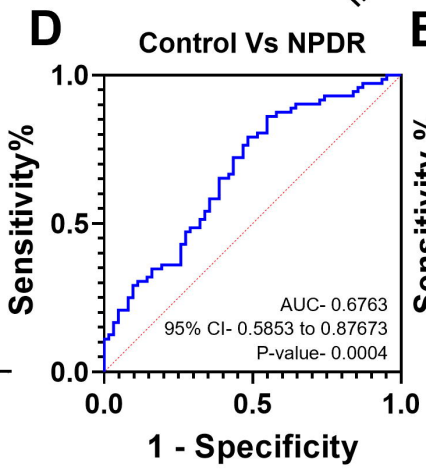
D
Control Vs NPDR
Sensitivity%
1.0
0.5
0.0
AUC- 0.6763
95% CI- 0.5853 to 0.87673
P-value- 0.0004
0.0
0.5
1.0
1 - Specificity

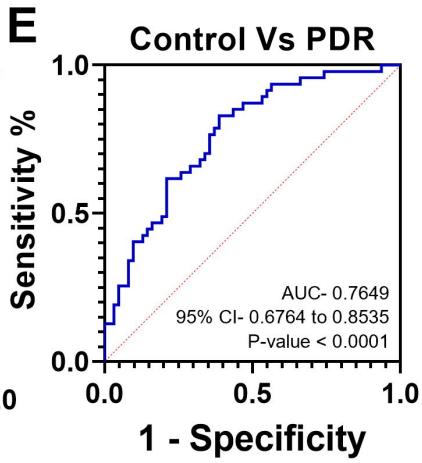
E
Control Vs PDR
Sensitivity %
1.0
0.5
0.0
AUC- 0.7649
95% CI- 0.6764 to 0.8535
P-value < 0.0001
0.0
0.5
1.0
1 - Specificity

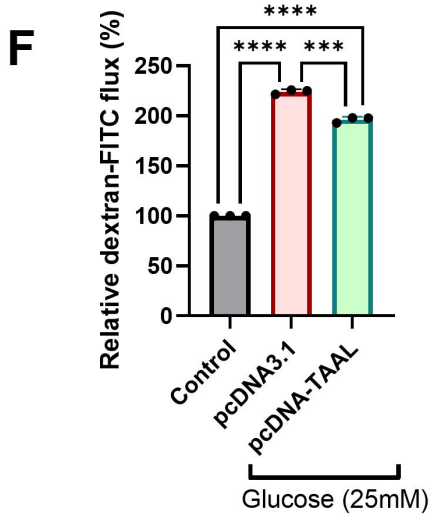
F
Relative dextran-FITC flux (%)
250
200
150
100
50
0
****
****
***
Control
pcDNA3.1
pcDNA-TAAL
Glucose (25mM)

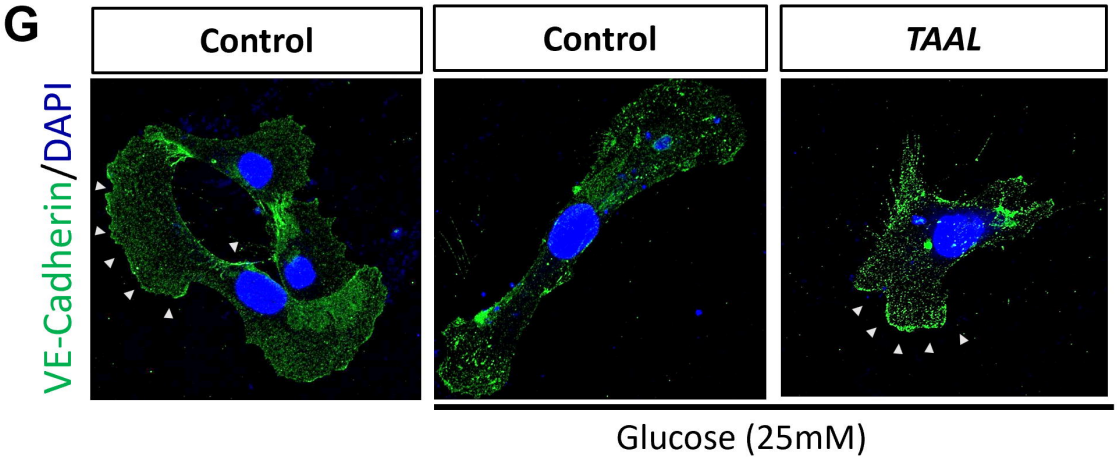
G
Control
Control
TAAL
VE-Cadherin/DAPI
Glucose (25mM)

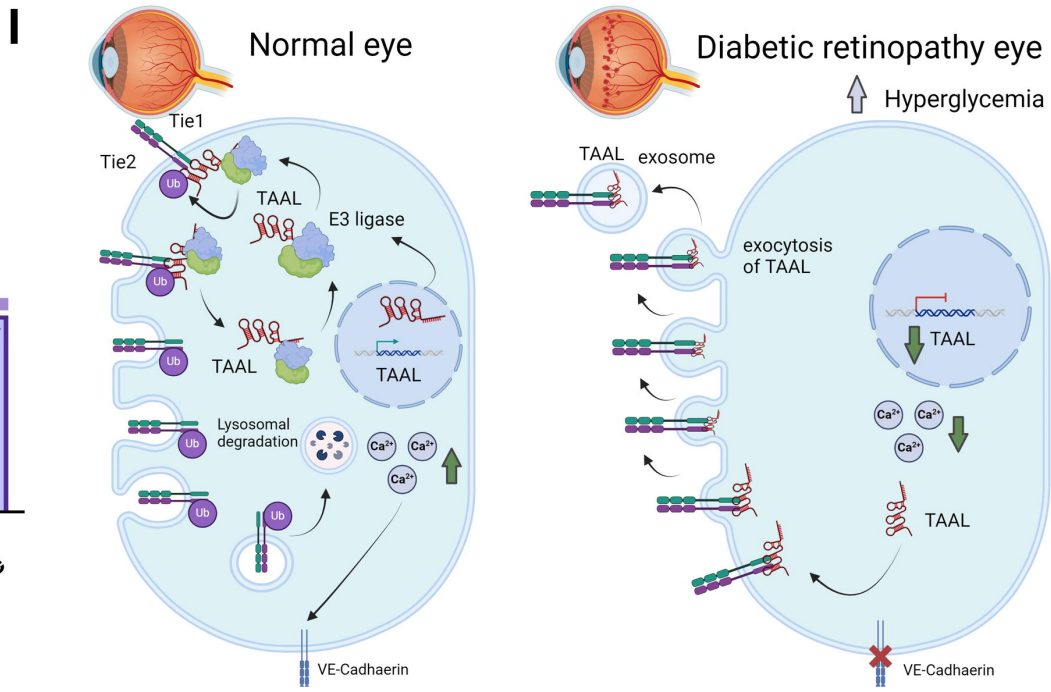
I
Normal eye
Tie1
Tie2
Ub
TAAL
E3 ligase
TAAL
TAAL
Lysosomal degradation
Ca2+
VE-Cadhaerin
Diabetic retinopathy eye
Hyperglycemia
TAAL
exosome
exocytosis of TAAL
TAAL
TAAL
VE-Cadhaerin

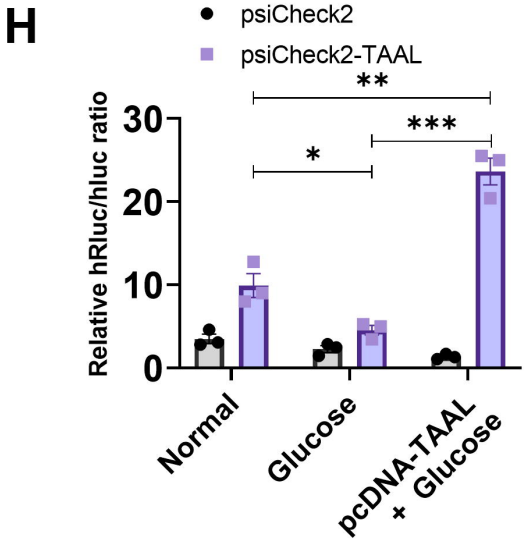
H
psiCheck2
psiCheck2-TAAL
Relative hRluc/hluc ratio
30
20
10
0
**
***
*
Normal
Glucose
pcDNA-TAAL + Glucose

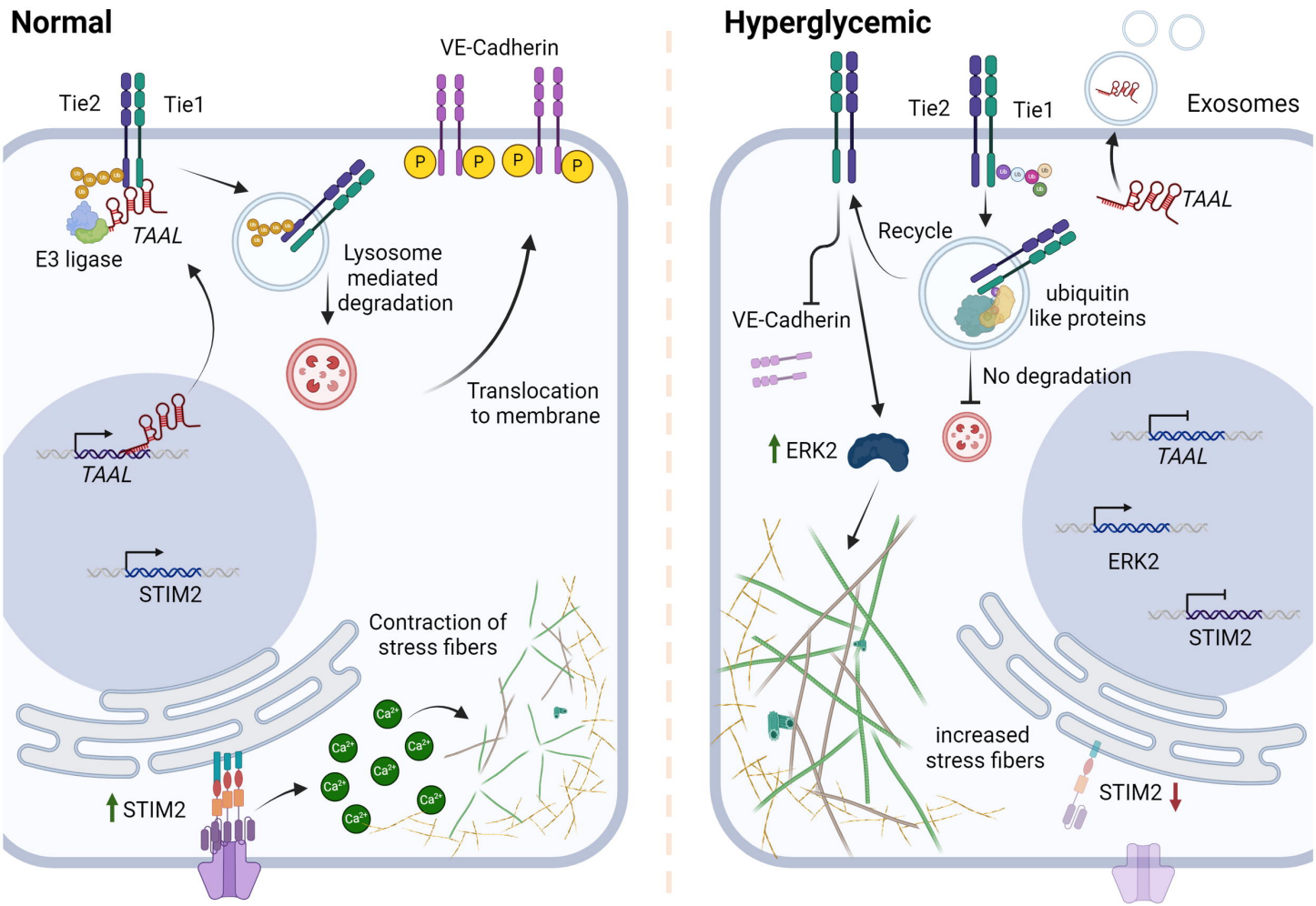
Normal
VE-Cadherin
Tie2
Tie1
P
P
P
P
TAAL
E3 ligase
Lysosome
mediated
degradation
Translocation
to membrane
TAAL
STIM2
Contraction of
stress fibers
Ca2+
STIM2
Hyperglycemic
Tie2
Tie1
Exosomes
TAAL
Recycle
ubiquitin
like proteins
VE-Cadherin
No degradation
ERK2
TAAL
ERK2
STIM2
increased
stress fibers
STIM2